Boise State University
ScholarWorks

Boise State Patents   The Albertsons Library

7-31-2012

Multi-State Memory and Multi-Functional Devices Comprising Magnetoplastic or Magnetoelastic Materials

Peter Müllner
Boise State University

William Knowlton
Boise State University

28 Claims, 13 Drawing Sheets

(54) **MULTI-STATE MEMORY AND MULTI-FUNCTIONAL DEVICES COMPRISING MAGNETOPLASTIC OR MAGNETOELASTIC MATERIALS**

(75) Inventors: **Peter Mullner**, Boise, ID (US); **William B Knowlton**, Boise, ID (US)

(73) Assignee: **Boise State University**, Boise, ID (US)

(*) Notice: Subject to any disclaimer, the term of this patent is extended or adjusted under 35 U.S.C. 154(b) by 0 days.

This patent is subject to a terminal disclaimer.

(21) Appl. No.: **12/773,831**

(22) Filed: **May 4, 2010**

(65) **Prior Publication Data**

US 2011/0110139 A1 May 12, 2011

Related U.S. Application Data

(63) Continuation of application No. 11/940,316, filed on Nov. 14, 2007, now Pat. No. 7,710,766.

(60) Provisional application No. 60/859,163, filed on Nov. 14, 2006.

(51) **Int. Cl.**
G11C 11/00 (2006.01)

(52) **U.S. Cl.** **365/157**; 365/145; 365/66; 365/225.5; 365/185.03
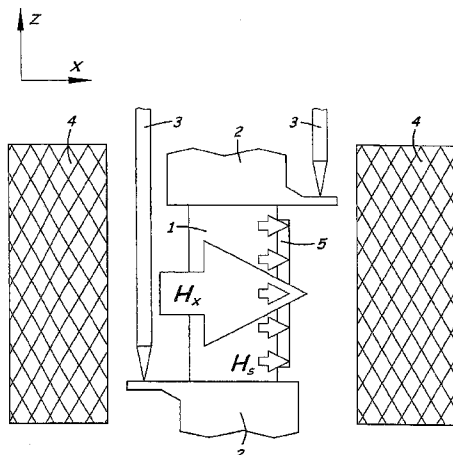
(58) **Field of Classification Search** 365/157, 365/145, 66, 225.5, 185.03
See application file for complete search history.

(56) **References Cited**

U.S. PATENT DOCUMENTS

3,288,942 A 11/1966 Voegeli
3,577,108 A 5/1971 Bengtson et al.
4,364,013 A 12/1982 Castera et al.

5,155,622 A * 10/1992 Kawatsuki et al. 359/485.03
(Continued)

FOREIGN PATENT DOCUMENTS

WO WO2008/049124 A2 4/2008
(Continued)

OTHER PUBLICATIONS

Chernenko VA, Cesari E, Kokorin VV, Vitenko IN, The Development of New Ferromagnetic Shape Memory Alloys in Ni-Mn-Ga System, Scripta Metal Mater 1995;33:1239.

(Continued)

Primary Examiner — Connie Yoha
(74) *Attorney, Agent, or Firm* — Pedersen and Company, PLLC; Ken J. Pedersen; Barbara S. Pedersen

(57) **ABSTRACT**

Apparatus and methods are disclosed that enable writing data on, and reading data of, multi-state elements having greater than two states. The elements may be made of magnetoplastic and/or magnetoelastic materials, including, for example, magnetic shape-memory alloy or other materials that couple magnetic and crystallographic states. The writing process is preferably conducted through the application of a magnetic field and/or a mechanical action. The reading process is preferably conducted through atomic-force microscopy, magnetic-force microscopy, spin-polarized electrons, magneto-optical Kerr effect, optical interferometry or other methods, or other methods/effects. The multifunctionality (crystallographic, magnetic, and shape states each representing a functionality) of the multi-state elements allows for simultaneous operations including read&write, sense&indicate, and sense&control. Embodiments of the invention may be used, for example, for storing, modifying, and accessing data for device, sensor, actuator, logic and memory applications. Embodiments may be particularly effective for non-volatile memory or other read&write, sense&indicate, and/or sense&control functions in computer or other applications; such simultaneous operation of two (or more) of said multiple functionalities open new pathways for miniaturization of devices.

28 Claims, 13 Drawing Sheets

U.S. PATENT DOCUMENTS

5,418,030 A *	5/1995	Tominaga et al.	.... 428/64.6
5,850,109 A	12/1998	Mock et al.	
5,952,094 A	9/1999	Van Kesteren et al.	
5,958,154 A	9/1999	O'Handley et al.	
6,034,887 A	3/2000	Gupta et al.	
6,037,682 A	3/2000	Shoop et al.	
6,307,241 B1	10/2001	Awschalom et al.	
6,433,465 B1	8/2002	McKnight et al.	
6,515,382 B1	2/2003	Ullakko	
6,655,035 B2	12/2003	Bent et al.	
6,909,224 B2	6/2005	Ghandi et al.	
6,927,475 B2	8/2005	Lu	
6,984,902 B1	1/2006	Huang et al.	
6,995,496 B1	2/2006	Hagood, IV et al.	
7,009,310 B2	3/2006	Cheung et al.	
7,020,015 B1	3/2006	Hong et al.	
7,059,201 B2	6/2006	Prakash et al.	
7,119,495 B2	10/2006	Jang	
7,177,121 B2 *	2/2007	Kojima et al.	.... 360/324.12
7,556,871 B2 *	7/2009	Ichihara et al.	.... 428/830
7,564,152 B1	7/2009	Clark et al.	
7,710,766 B2 *	5/2010	Mullner et al.	.... 365/157
2004/0160846 A1	8/2004	Rinerson et al.	
2004/0264229 A1	12/2004	Tsu	
2005/0050258 A1	3/2005	Frommer et al.	
2006/0003185 A1	1/2006	Parkin	
2006/0130758 A1	6/2006	Lohokare et al.	
2006/0222904 A1	10/2006	Hsia et al.	
2007/0267596 A1	11/2007	Husmann et al.	
2008/0143195 A1	6/2008	Hampikian et al.	
2008/0180991 A1	7/2008	Wang	
2008/0225575 A1	9/2008	Mullner et al.	
2008/0246104 A1	10/2008	Ranjan et al.	
2009/0092817 A1	4/2009	Mullner et al.	
2009/0167115 A1	7/2009	Tucker et al.	

FOREIGN PATENT DOCUMENTS

WO	WO2008/061166 A3	5/2008	
WO	WO2009/029953 A2	3/2009	

OTHER PUBLICATIONS

Chernenko VA, L'Vov VA, Pasquale M, Besseghini S, Sasso C, Polenur DA, Magnetoelastic Behavior of Ni-Mn-Ga Martensitic Alloys, Int J Appl Electromag Mech 2000;12:3.

Chernenko VA, Müllner P, Wollgarten M, Pons J, Kostorz G, Magnetic Field Induced Strains Caused by Different Martensites in Ni-Mn-Ga Alloys, J de Phys IV, 2003;112:951.

Ferreira PJ, Vander Sande JB, Magnetic Field Effects on Twin Dislocations, Scripta Mater 1999;41:117.

Jääskeläinen A, Ullakko K, Lindroos VK, Magnetic Field-Induced Strain and Stress in a Ni-Mn-Ga Alloy, J de Phys IV, 2003;112:1005.

Murray SJ, Marioni M, Allen SM, O'Handley RC, Lograsso TA, 6% Magnetic-Field-Induced Strain by Twin-Boundary Motion in Ferromagnetic Ni-Mn-Ga, Appl Phys Lett 2000a;77:886.

Murray SJ, Marioni M, Kukla AM, Robinson J, O'Handley RC, Allen SM, Large Field Induced Strain in Single Crystalline Ni-Mn-Ga Ferromagnetic Shape Memory Alloy, J Appl Phys 2000b;87:5774.

Müllner P, Between Microscopic and Mesoscopid Descriptions of Twin—Twin Interaction, Int J Mater Res (Z f Metallk) 2006;97:205.

Müllner P, Chernenko VA, Wollgarten M, Kostorz G, Large Cyclic Deformation of a Ni-Mn-Ga Shape Memory Alloy Induced by Magnetic Fields, J Appl Phys 2002;92:6708.

Müllner P, Chernenko VA, Kostorz G, A Microscopic Approach to the Magnetic-Field-Induced Deformation of Martensite (Magnetoplasticity), J Magn Magn Mater 2003a;267:325.

Müllner P, Chernenko VA, Kostorz G, Stress-Induced Twin Rearrangement Resulting in Change of Magnetization in a Ni-Mn-Ga Ferromagnetic Martensite, Scripta Mater 2003b;49:129.

Müllner P, Chernenko VA, Kostorz G, Large Magnetic-Field-Induced Deformation and Magneto-Mechanical Fatigue of Ferromagnetic Ni-Mn-GA Martensites, Mater Sci Eng A 2004;387:965.

Müllner P, Ullakko K, The Force of a Magnetic/Electric Field on a Twinning Dislocation, Phys Stat Sol (b) 1998;208:R1.

Pond RC, Celotto S, Special Interfaces: Military Transformations, Intern Mater rev 2003;48:225.

Sozinov A, Likhachev AA, Lanska N, Ullakko K, Giant Magnetic-Field-Induced Strain in NiMnGa Seven-Layered Martensitic Phase, Appl Phys Lett 2002;80:1746.

Straka L, Heczko O, Magnetization Changes in Ni-Mn-Ga Magnetic Shape Memory Single Crystal During Compressive Stress Reorientation, Scripta Mater 2006;54:1549.

Soursa I, Pagounis E, Ullakko K, Magnetization Dependence on Strain in the Ni-Mn-Ga Magnetic Shape Memory Material, Appl. Phys. Lett. 2004a; 23:4658.

Suorsa I, Tellinen J, Ullakko K, Pagounis E, Voltage Generation Induced by Mechanical Straining in Magnetic Shape Memory Materials, J Appl Phys 2004b;95:8054.

Tickle R, James RD, Magnetic and Magnetomechanical Properties of Ni2MnGa, J Magn Magn Mater 1999;195:627.

.Ullakko K, Magnetically Controlled Shape Memory Alloys: A New Class of Actuator Materials, J Mater Eng Perf, 1996;5:405.

Ullakko K, Huang JK, Kantner C, O'Handley RC, Kokorin VV, Large Magnetic-Field-Induced Strains in Ni2MnGa Single Crystals, J Appl Phys 1996;69:1966.

Likhachev et al., Magnetic-field-cotrolled twin boundaries motion and giant magneto-mechanical effects in Ni-Mn-Ga shape memory alloy, Physics Letters, Oct. 2, 2000, pp. 142-151, vol. A 275, Elsevier Science.

Li et al., Some aspects of strain-induced change of magnetization in a Ni-Mn-Ga single crystal, Scripta Materialla, available online Jul. 6, 2005, pp. 829-834, vol. 53, Elsevier Ltd.

Boonyongmaneerat et al., Increasing Magnetoplasticity in Polycrystalline Ni-Mn-Ga by Reducing Internal Constraints through Porosity, Physical Review Letters, Dec. 14, 2007, pp. 247201-1 to 247201-4, vol. 99, The American Physical Society.

PCT Search Report and the Written Opinion, PCT/US07/82021, May 21, 2008, Applicant: Boise State University.

PCT Search Report and the Written Opinion, PCT/US37/84732, May 22, 2008, Applicant: Boise State University.

PCT Search Report, PCT/US2008/075062, May 18, 2009, Applicant: Boise State University.

Wang, et al., Energy harvesting by magnetostrictive materials (MsM) for powering wireless sensors in SHM, SPIE/ ASME Best Student Paper Presentation Contest, SPIE Smart Structures and Materials and NDE and Health Monitoring, 14th International Symposium (SSNo7), Mar. 18-22, 2007.

Karaman et al., Energy harvesting using martensite variant reorientation mechanism in a NiMnGa magnetic shape memory alloy, Applied Physics Letters, 90, 172505 (2007).

Chernenko, et al., Martensite transformation in ferromagnets: experiment and theory, J Magn Mater 1990;16-197; 859.

J. Cui, T. W. Shield, R. D. James, Phase transformation and magnetic anisotropy of an iron-palladium ferromagnetic shape-memory alloy, Acta mater. 52, 35 (2004).

A. Fujita, K. Fukamichi, F. Gejima, R. Kainuma, K. Ishida, Magnetic properties and large magnetic-field-induced induced strains in off-stoichiometric Ni-Mn-Al Heusler alloys, Appl. Phys. Lett. 77, 3054 (2000).

R. D. James and M. Wuttig, Magnetostriction of martensite, Phil. Mag. A 77, 1273 (1998).

G. Kostorz and P. Müllner, Z. F., Magnetoplasticity, Metallkd. 96, 703 (2005).

H. H. Liebermann and C. D. Graham, Jr., Plastic and Magnetoplastic Deformation of Dy Single Crystals, Acta Met. 25, 715 (1976).

R. Santamarta, E. Cesari, J. Font, J. Muntasell, J. Pons, J. Dutkiewicz, Effect of atomic order on the martensitic transformation of Ni-Fe-Ga alloys, Scripta Mater. 54, 1985 (2006).

A. S. Sologubenko, P. Müllner, H. Heinrich, K. Kostorz, Z. F., On the plate-like-phase formation in MnAl-C alloys, Metallkd. 95, 486 (2004).

N. I. Vlasova, G. S. Kandaurova, N. N. Shchegoleva, J., Effect of the polytwinned microstructure parameters on magnetic domain structure and hysteresis properties of the CoPt-type alloys, Magn. Magn. Mater. 222, 138 (2000).

T. Wada, T. Tagawa, M. Taya, Martensitic transformation in Pd-rich Fe-Pd-Pt alloy, Scripta Mater. 48, 207 (2003).

M. Wuttig, J. Li, C. Craciunescu, A New Ferromagnetic Shape Memory Alloy System, Scripts Mater. 44, 2393 (2001).

J. H. Zhang, W. Y. Peng, S. Chen, T.Y. Hsu (X. Zaoyao), Magnetic shape memory effect in an antiferromagnetic-Mn-Fe(Cu) alloy, Appl. Phys. Lett. 86, 022506 (2005).

Mullner et al., Large cyclic magnetic-field-induced deformation in orthorhombic (14M) Ni-Mn-Ga martensite, Journal of Applied Physics, Feb. 1, 2004, pp. 1531-1536, vol. 95, No. 3, American Institute of Physics.

Mullner et al., Nanomechanics and magnetic structure of orthorhombic Ni-Mn-Ga martensite, Materials Science & Engineering A, 2008, pp. 66-72, 481-482, Eslevier.

Mullner et al., Micromechanics of magnetic-field-induced twin-boundary motion in Ni-Mn-Ga magnetic shape-memory alloys, Solid-to-Solid Phase Transformations in Inorganic Materials, May 29-Jun. 3, 2005, pp. 171-185, vol. 2, TMS (The Minerals, Metals & Materials Society).

Mullner et al., The force of a magnetic/electric field on a twinning dislocation, Phys. Stat. Sol. (b), 1998, pp. R1-R2, 208, Rapid Research Notes.

Pan et al., Micromagnetic study of Ni2MnGa under applied field (invited), Journal of Applied Physics, May 1, 2000, pp. 4702-4706, vol. 87, No. 9, American Institute of Physics.

Sozinov et al., Crystal structures and magnetic anisotropy properties of Ni-Mn-Ga Martensitic phases with giant magnetic-field-induced strain, IEEE Transactions on Magnetics, Sep. 2002, pp. 2814-2816, vol. 38, No. 5, IEEE.

Sullivan, et al., Temperature- and field-dependent evolution of micromagnetic structure in ferromagnetic shape-memory alloys, Physical Review B, 2004, pp. 1-8, 70:094427, The American Physical Society.

Ge et al., Various magnetic domain structures in a Ni-Mn-Ga martensite exhibiting magnetic shape memory effect, Journal of Applied Physics, Aug. 15, 2004, pp. 2159-2163, vol. 96, No. 4, American Institute of Physics.

Greer et al., Size dependence of mechanical properties of gold at the micron scale in the absence of strain gradients, Acta Materialia, 2005, pp. 1821-1830, 53, Elsevier.

Jaaskelainen et al., Magnetic field-induced strain and stress in a Ni-Mn-Ga alloy, J. Phys. IV, 2003, 112, 1005, EDP Sciences (Abstract only).

Murray et al., 6% magnetic-field-induced strain by twin-boundary motion in ferromagnetic Ni-Mn-Ga, Applied Physics Letters, Aug. 7, 2000, pp. 886-888, vol. 77, No. 6, American Institute of Physics.

Murray et al., Large field induced strain in single crystalline Ni-Mn-Ga ferromagnetic shape memory alloy, Journal of Applied Physics, May 1, 2000, pp. 5774-5776, vol. 87, No. 9, American Institute of Physics.

Tellinen et al., Basic properties of magnetic shape memory actuators, www.adaptamat.com, "Actuator 2002", Jun. 10-12, 2002, Bremen, Germany.

Suorsa et al., Applications of magnetic shape memory actuators, www.adaptamat.com, "Actuator 2002", Jun. 10-12, 2002, Bremen, Germany.

Lundgren et al., A magnetostrictive electric generator, IEEE Transaction on Magnetics, Nov. 1993, pp. 3150-3152, vol. 29, No. 6, IEEE.
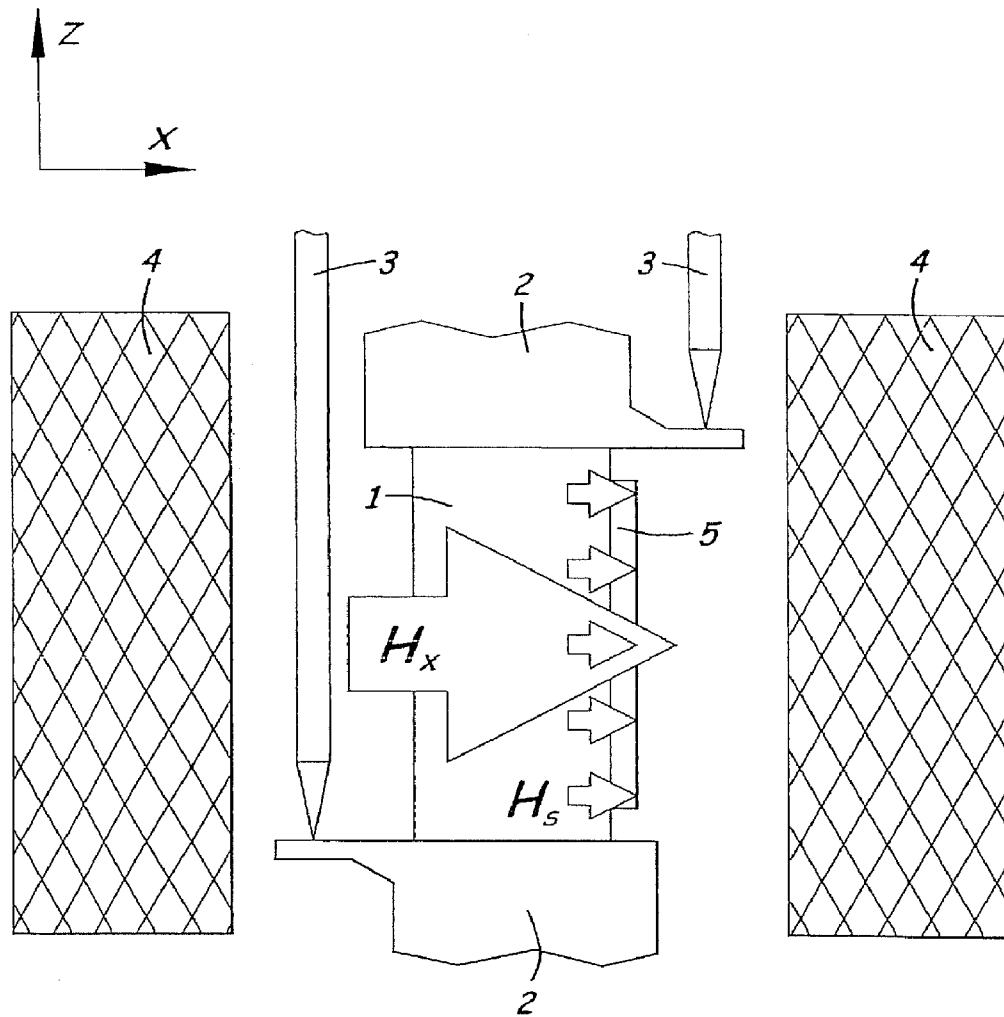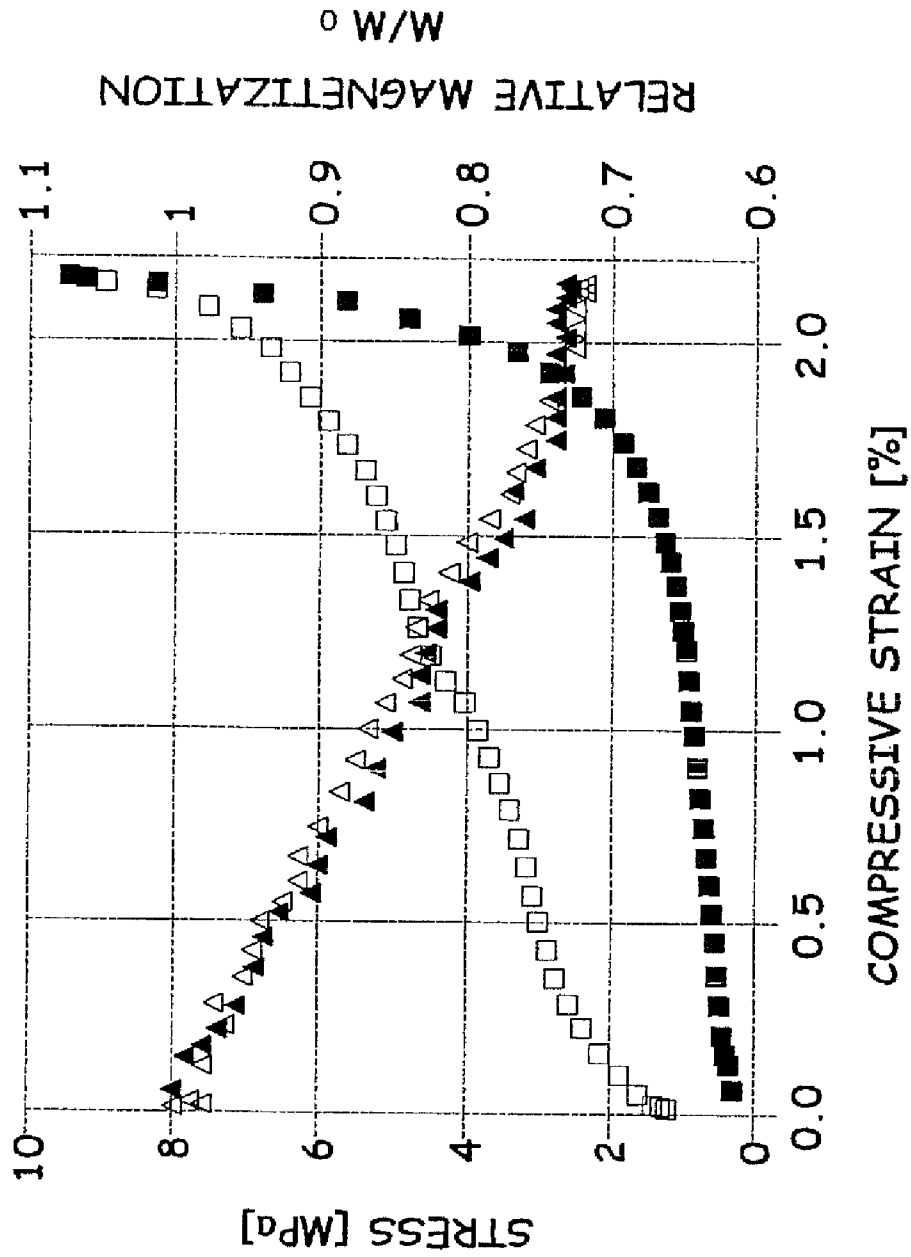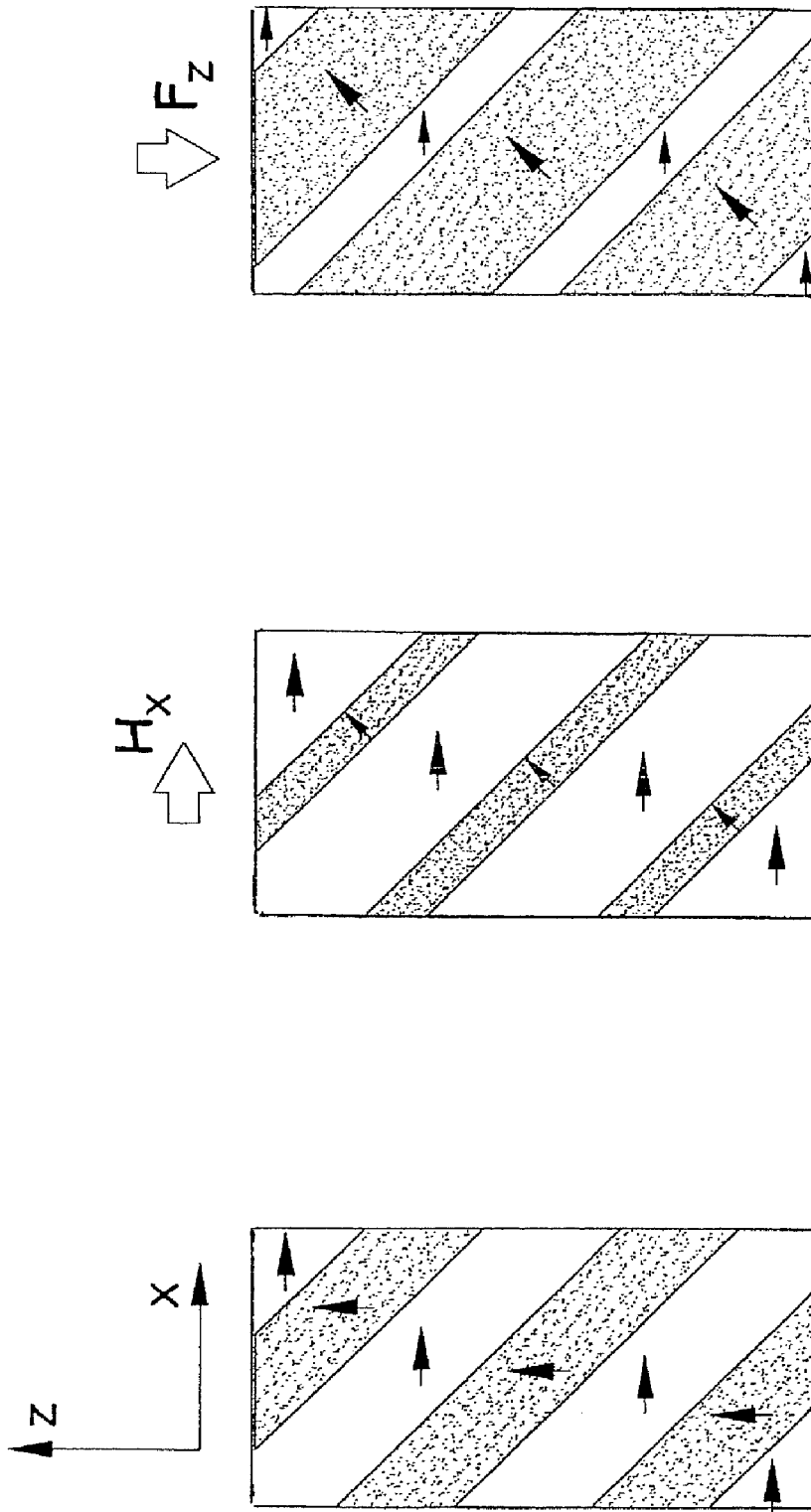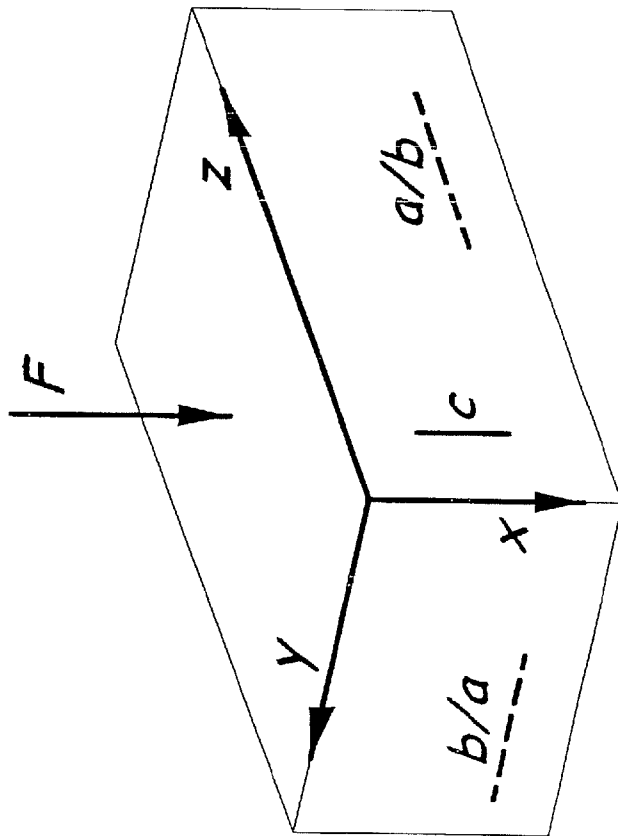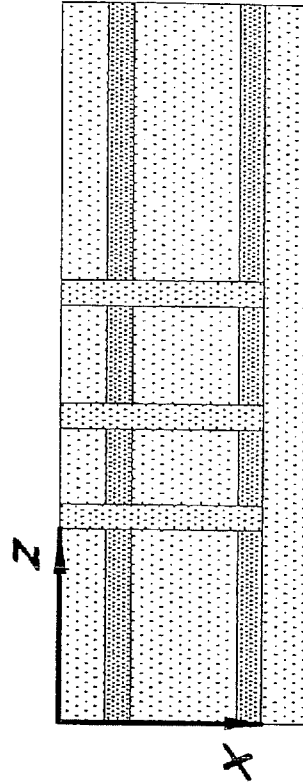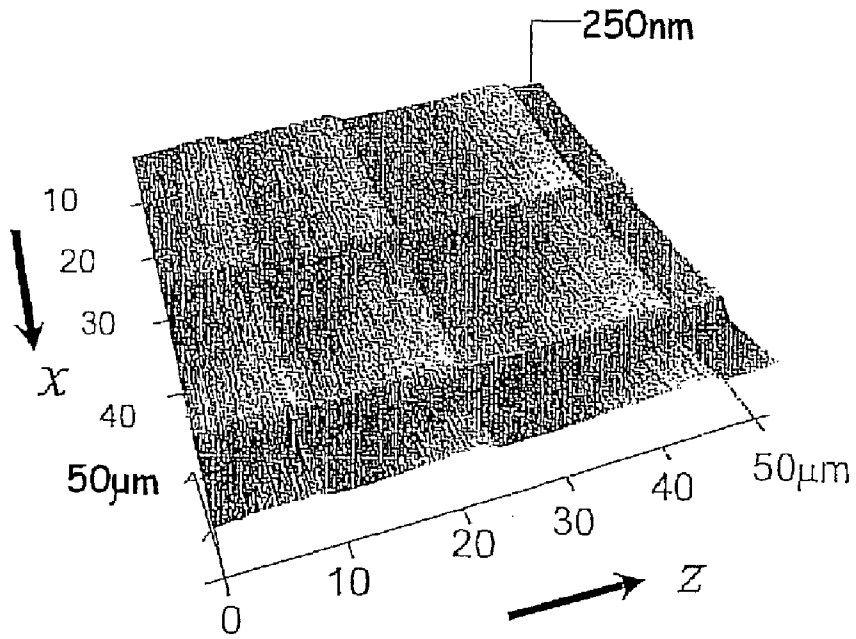
* cited by examiner

Fig. 1

Fig. 2

Fig. 3C

Fig. 3B

Fig. 3A

Fig. 4B

Fig. 4A

250nm

10
20
30

x

40

50μm

0   10   20   30   40   50μm

z

Fig. 5

z

B   A

x

c c

_a_   _b_

b C

_a_
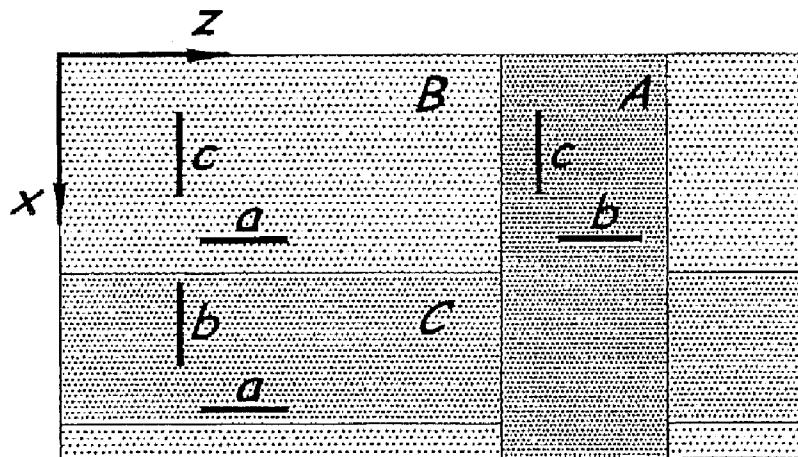
Fig. 7
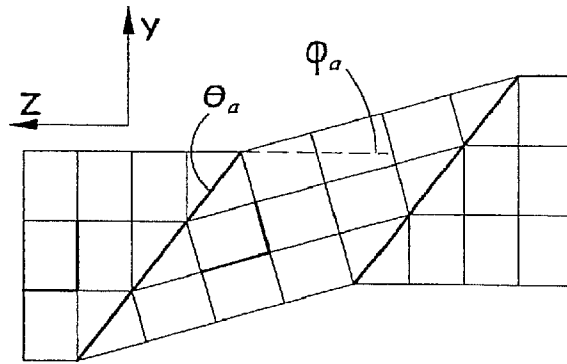
Fig. 6A
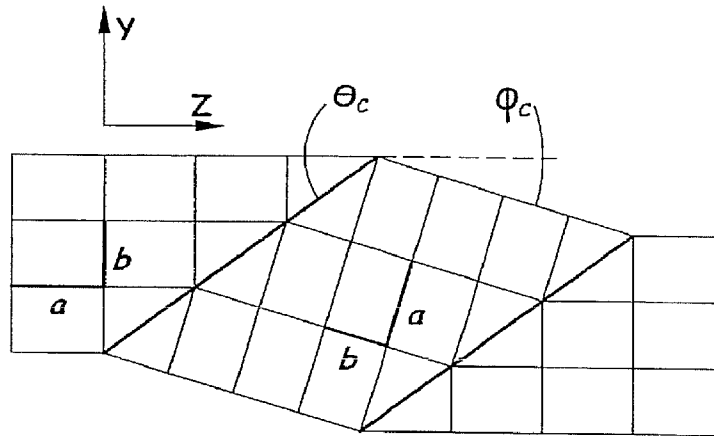
Fig. 6B
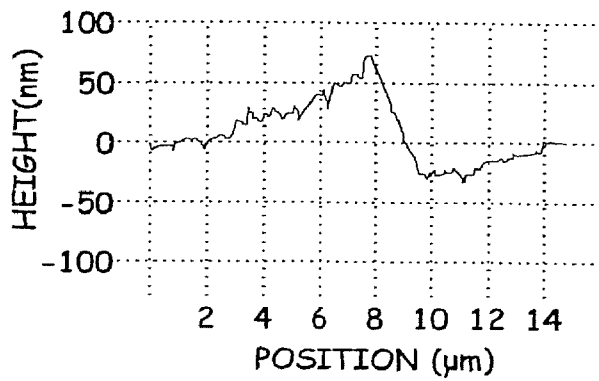
Fig. 6C
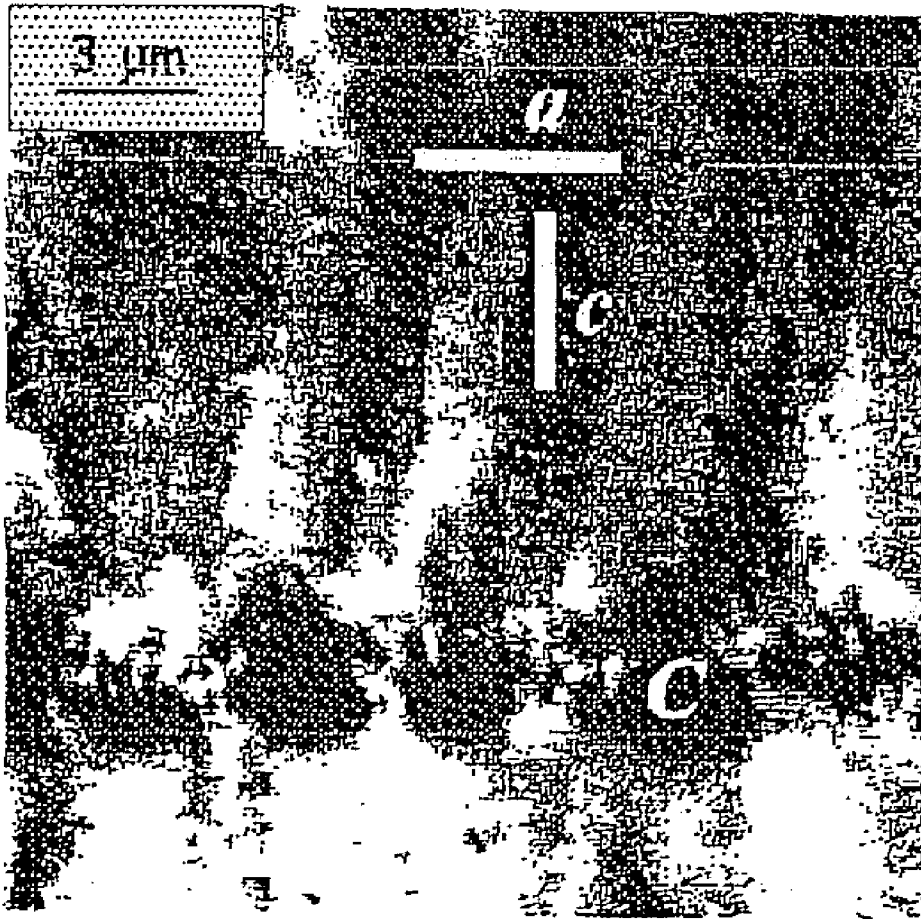
Fig. 8B
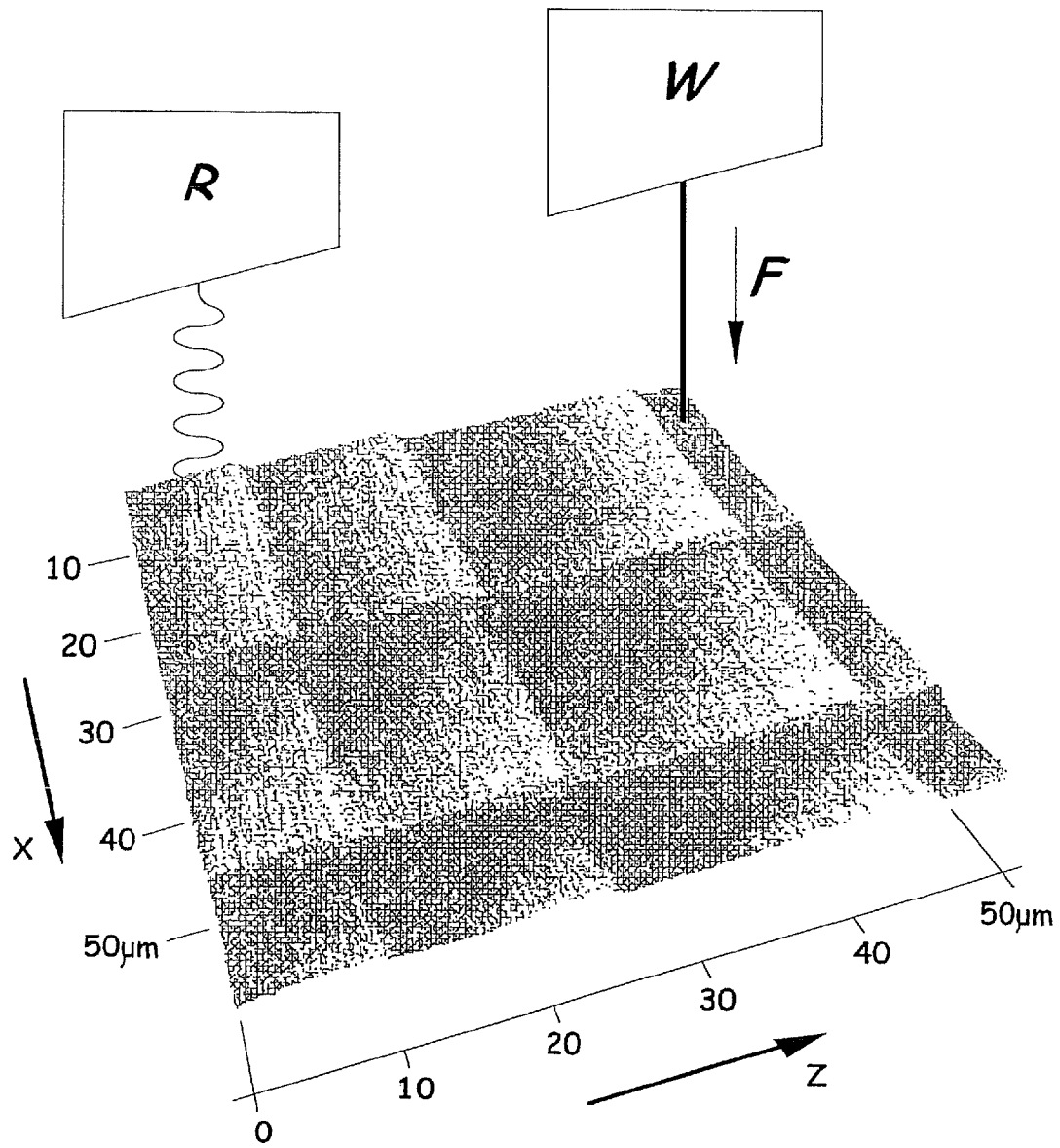
Fig. 9

	K [MJ/m³]	M_S [MA/m]	$\tau_{M,max}$ [MPa]	$\varepsilon_{M,max}$ [%]	$\mu_0 H_a$ [T]
Ni₂MnGa	0.25	0.5	2	10	1
Dy	44	3.0	220	10	30
α-Fe	0.05	1.1	0.07	35	0.06
Co-Ni	0.7	1.0	2	18	1.4
τ-MnAl C	1	0.5	1.4	35	4
L1₀ FePd	2.2	1.0	3	35	4
L1₀ CoPt	4.9	0.8	7	35	12
L1₀ FePt	6.6	1.1	9	35	12

Fig. 10

CATEGORY	MATERIAL	REFERENCE
HEUSLER SHAPE-MEMORY ALLOY	Ni_2MnGa	[KOSTORZ 2005]
	Co_2NiGa	[WUTTIG 2001]
	Ni_2MnAl	[FUJITA 2000]
	Ni_2FeGa	[SANTA 2006]
NON-HEUSLER FERROMAGNETIC SHAPE-MEMORY ALLOY	Fe_3Pd	[JAMES 1998]
		[CUI 2004]
	Fe-Pd-Pt	[WADA 2003]
	$L1_0CoPt$	[VLASOVA 2000]
ANTIFERROMAGNETIC SHAPE-MEMORY ALLOY	γ-Mn-Fe-Cu	[ZHANG 2005]
NON SHAPE-MEMORY ALLOY	Dy	[LIEB. 1976]
	τ-MnAl-C	[SOLO. 2004]

Fig. 11

FIG 12

Fig. 13A

Fig. 13B

MULTI-STATE MEMORY AND MULTI-FUNCTIONAL DEVICES COMPRISING MAGNETOPLASTIC OR MAGNETOELASTIC MATERIALS

This application is a continuation of U.S. Non-Provisional application Ser. No. 11/940,316, filed Nov. 14, 2007, and issuing on May 4, 2010 as U.S. Pat. No. 7,710,766, which claims benefit of U.S. Provi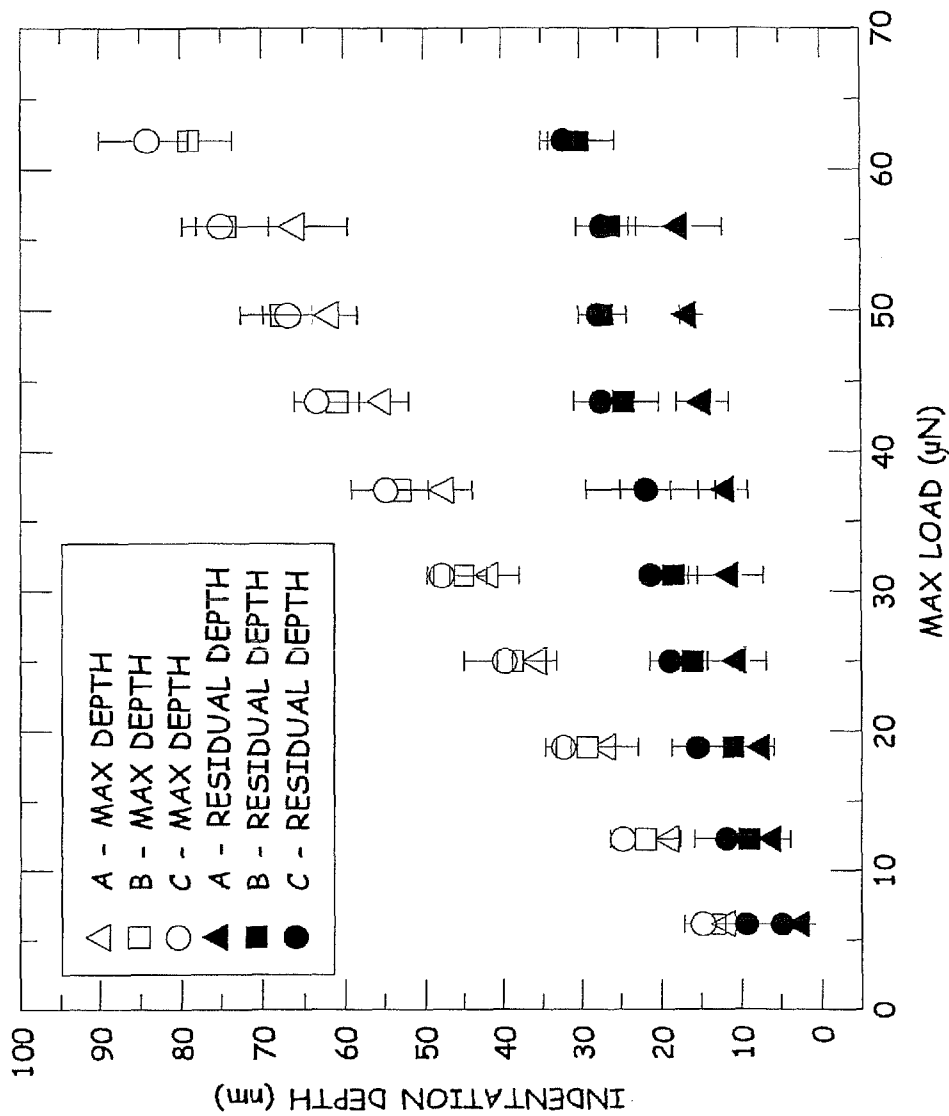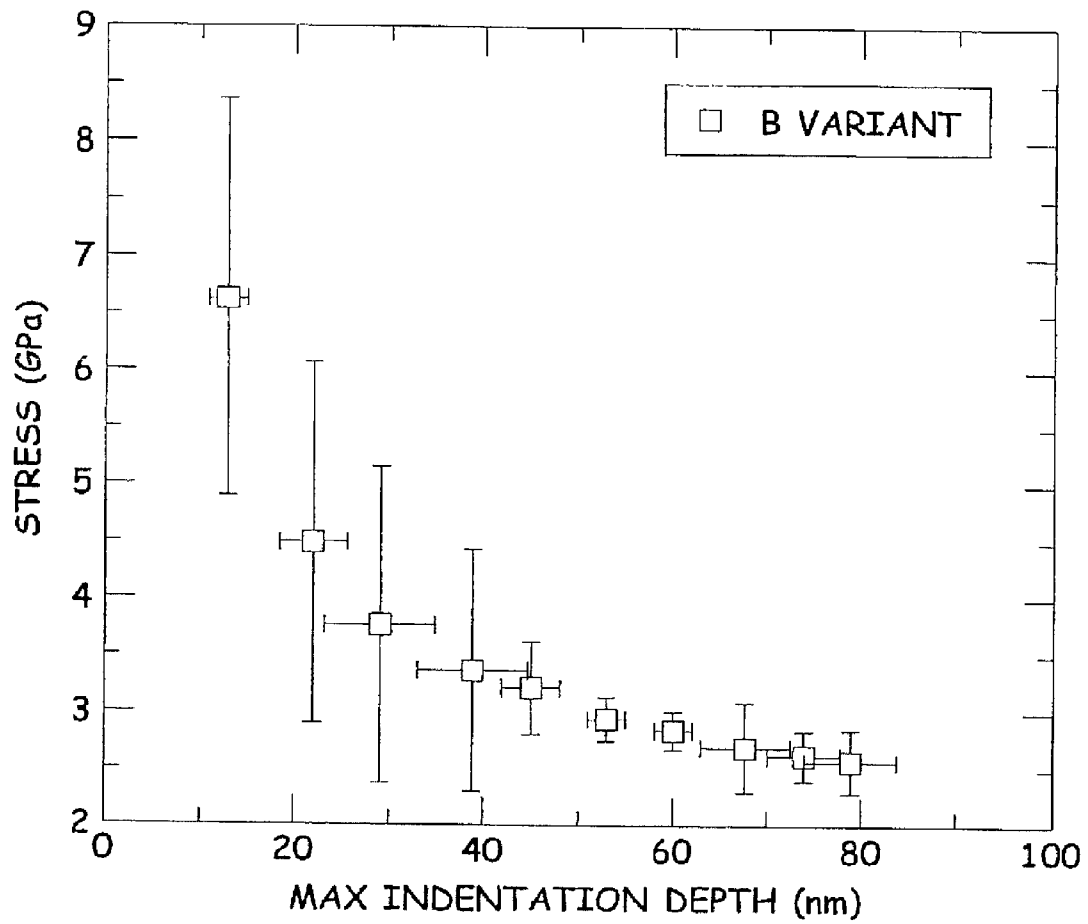sional Application 60/859,163, filed Nov. 14, 2006, the entire disclosures of which are incorporated herein by reference

FIELD OF THE INVENTION

The invention relates to multi-state memory and/or multi-functional devices using magnetoplastic and/or magnetoelastic materials, which couple magnetic and crystallographic/shape states. More specifically, the present invention relates to crystallographic and magnetic states of magnetoplastic and/or magnetoelastic materials, including magnetic shape memory alloys (MSMA) and other materials, to store, access, and modify data for sensor, actuator, logic and memory applications.

Current conventional logic, memory, and sensing and control technology is based on binary elements. Typically, a binary element contains semiconductor material that has two states, a conducting one, and an insulating one. On the other hand, the present invention relates to devices and methods wherein elements made of magnetoplastic and/or magnetoelastic materials are used, said elements preferably having six crystallographic states, and wherein the crystallographic states are linked to three magnetic states. This enables the combined usage of a single element as memory and logical unit. As a consequence, the low-level programming of computers becomes much more efficient. Because a single element may have six states (rather than two), memory density increases 3 fold. Because each of the six states are stable without the use of an external force (e.g., without external electric field or other continued force), the memory provided by said element can be nonvolatile.

Magnetoplastic materials, including ferromagnetic shape-memory alloys with twinned martensite, tend to deform upon the application of a magnetic field (Ullakko 1996, Murray et al. 2000, Chernenko et al. 2000). The magnetic-field-induced deformation can be irreversible (magnetoplasticity, Mullner et al. 2002, Mullner et al. 2003 a) or reversible (magnetoelasticity, Chernenko et al. 2000, Ullakko et al. 1996). The magnetoplastic effect is related to the magnetic-field-induced displacement of twin boundaries, in an irreversible process. The magnetoelastic effect is also related to the magnetic-field-induced displacement of twin boundaries, but in a process that is at least somewhat reversible. While a strict definition of "elastic" would imply that magnetoelastic materials return without hysteresis to their initial state after removal of the magnetic-field, the term "magnetoelastic," as it is frequently used, may include materials that deform and return to their initial state upon removal of the magnetic field either without hysteresis or with some hysteresis.

While literature on the subject of magnetoplasticity and magnetoelasticity has indicated such materials to be relevant as actuators for converting electrical energy, or changes in magnetic field, to mechanical motion, the invention utilizes, in combination, magnetoplasticity/magnetoelasticity and the reverse or inverse effect (strain-induced change of magnetization) for data reading and writing, which may take the forms of memory and retrieval, displacement and sensing, sensing and control, or sensing and indicating, for example.

The inventors believe that magnetoplastic and/or magnetoelastic materials are uniquely suitable as multi-state data storage devices due to their large range of deformation, small threshold stress and significant change of magnetization. See Mullner et al 2003b, Straka and Heczko 2006, Suorsa et al. 2004, below, for discussions of range of deformation, threshold stress, and change of magnetization for magnetoplastic materials.

Closed-loop control of any automated process, including machines and robots, contains three main elements: a motor/actuator that drives the tool, a sensor that detects the position of the tool, and a controller that activates the motor. Sensor and controller are linked through elaborate electronics. In view of miniaturization, the electronics become a limiting aspect of the system. Multifunctional multi-state devices, according to embodiments of the invention, are a pathway to overcome these limitations by inherently linking them between magnetic and crystallographic and/or shape states, wherein one function utilizing said multi-states will operate as a sensing means and the other function utilizing said multi-states will operate as control signal means. Similarly, displace&sense, sense&indicate, and read&write operations (such as memory storage and retrieval) are sets of functions that can be performed sequentially or simultaneously by causing/urging/actuating the material to enter various different magnetic and crystallographic and/or shape states (herein called "writing"), and then sensing/responding to said various different magnetic and crystallographic and/or shape states (herein called "reading").

RELATED ART

Background references that may be relevant to embodiments of the invention include:

Chemenko V A, Cesari E, Kokorin V V, Vitenko I N, Scripta Metal Mater 1995; 33:1239.

Chernenko V A, L'vov V A, Cesari E, J Magn Magn Mater 1999; 196-197:859.

Chernenko V A, L'vov V A, Pasquale M, Besseghini S, Sasso C, Polenur D A, Int J Appl Electromag Mech 2000; 12:3.

Chernenko V A, Müllner P, Wollgarten M, Pons J, Kostorz G, J de Phys IV, 2003; 112:951.

Ferreira P J, Vander Sande J B, Scripta Mater 1999; 41:117.

Ge Y, Heczko O, SŘderberg O, Lindroos V K, J. Appl. Phys 2004; 96: 2159.

Greer J R, Oliver W C, Nix W D, Acta Mater 2005; 53:1821.

Jääskeläinen A, Ullakko K, Lindroos V K, J de Phys IV, 2003; 112:1005.

Murray S J, Marioni M, Allen S M, O'Handley R C, Lograsso T A, Appl Phys Lett 2000a; 77:886.

Murray S J, Marioni M, Kukla A M, Robinson J, O'Handley R C, Allen S M, J Appl Phys 2000b; 87:5774.

Müllner P, Int J Mater Res (Z f Metallk) 2006; 97:205.

Müllner P, Chernenko V A, Wollgarten M, Kostorz G, J Appl Phys 2002; 92:6708.

Müllner P, Chernenko V A, Kostorz G, J Magn Magn Mater 2003a; 267:325.

Müllner P, Chernenko V A, Kostorz G, Scripta Mater 2003b; 49:129.

Müllner P, Chernenko V A, Kostorz G, Mater Sci Eng A 2004a; 387:965.

Müllner P, Chernenko V A, Kostorz G, J Appl Phys 2004b; 95:1531.

Müllner P, Mukheiji D, Erni R, Kostorz G, Proc Int Conf "Solid to solid phase transformations in inorganic materials" PTM'05, Phoenix, Ariz., Mai 29-Jun. 3, 2005, Vol. 2:171.

Müllner P, Ullakko K, Phys Stat Sol (b) 1998; 208:R1.

Pan Q, James RD, J Appl Phys 2000; 87:4702.

Pond R C, Celotto S, Intern Mater rev 2003; 48:225.

Sozinov A, Likhachev A A, Lanska N, Ullakko K, Appl Phys Lett 2002; 80:1746.

Sozinov A, Ullakko K, IEEE Trans Magn 2002; 38:2814.

Straka L, Heczko O, Scripta Mater 2006; 54:1549.

Sullivan M R, Chopra H D, Phys Rev B 2004; 70:094427.

Suorsa I, Pagounis E, Ullakko K, Appl. Phys. Lett. 2004a; 23:4658.

Suorsa I, Tellinen J, Ullakko K, Pagounis E, J Appl Phys 2004b;95:8054.

Tickle R, James RD, J Magn Magn Mater 1999; 195:627.

Ullakko K, J Mater Eng Perf, 1996; 5:405.

Ullakko K, Huang J K, Kantner C, O'Handley R C, Kokorin V V, J Appl Phys 1996; 69:1966.

Ullakko K, Aaltio I, www.adaptamat.com, "Actuator 2002", Bremen, Germany.

Vlasova N I, Kandaurova G S, Shchegoleva N N, J Magn Magn Mater 2000; 222:138.

SUMMARY OF THE INVENTION

Apparatus and methods are proposed that comprise writing and reading of multi-state "bits" or multi-state elements on magnetoplastic and/or magnetoelastic materials or other materials that have greater than two magnetic, crystallographic, and/or shape states. Said "bits" or "elements" refer to individual/single portions/regions of material each adapted for receiving and holding information (writable) and also for said information being read (readable), and wherein "bit" is not intended to refer to traditional binary coding. "Multi-state" refers to greater than two states, and the multi-state bits/elements of the preferred embodiments are formed or defined by the magnetic and crystallographic/shape states of magnetoplastic and/or magnetoelastic materials Preferred embodiments of the invention may achieve multi-functionality by the multiple crystallographic, magnetic, and shape states of the bits/elements of the magnetoplastic/magnetoelastic materials, which allows for simultaneous operations including read&write, sense&indicate, and sense&control. Simultaneous operation of two (or more) functionalities open new pathways for miniaturization of devices.

The preferred writing process is conducted through the application of a magnetic field and/or a mechanical action to said magnetoplastic and/or magnetoelastic materials. It has been shown that switching magnetic/crystallographic domains changes the orientation of the surface of these materials. The surface inclination can be detected using light of any wave length and by using other forms of radiation. Thus, light and other forms of radiation may be used for the reading process. For example, the reading process may be conducted through atomic-force microscopy, magnetic-force microscopy, spin-polarized electrons, magneto-optical Kerr effect, optical interferometry or other methods, or a combination of the above.

BRIEF DESCRIPTION OF THE DRAWINGS

FIG. 1 is a schematic depiction of the experimental device with which deformation-induced change of magnetization was demonstrated.

FIG. 2 is a graph of stress and magnetization of a $Ni_{51}Mn_{28}Ga_{21}$ crystal as a function of compressive deformation in the device depicted in FIG. 1.

FIGS. 3 (a), (b), and (c) is a schematic depiction of the magnetization process through deformation in magnetoplastic martensitic materials.

FIGS. 4 (a) and (b) is a schematic depiction of a compressed/indented crystal sample.

FIG. 5 is a detail of the shaded face of the sample depicted in FIG. 4(a).

FIGS. 6 (a) and (b) is a schematic depiction of how twin crystallography is identified. FIG. 6(c) is a graphic depiction of an example atomic-force microscopy (AFM) surface profile relating to the angles ϕ_a and ϕ_c from FIG. 6(b).

FIG. 7 is a schematic depiction of how crystallographic twin variants are identified.

FIG. 8(a) is a depiction of a magnetic-force microscopy (MFM) result on the same area displayed in the shaded face (x-z plane) in FIGS. 4(a and b) and in FIG. 5. FIG. 8(b) is a magnified view of an area of FIG. 8(a) indicating an interaction of the domains across twin boundaries.

FIG. 9 is a schematic portrayal of one embodiment of the invention, wherein simultaneous writing and reading is performed on the sample of FIGS. 4 and 5.

FIG. 10 is a table of magnetic and magneto-mechanical properties of some but not all (potentially) ferromagnetic materials. Values surrounded by a rectangle being least favorable, and values surrounded by a triangle being most favorable.

FIG. 11 lists and categorizes many, but not all, magnetoplastic and potentially magnetoplastic materials, as well as citations to scientific literature discussing these materials. For materials that are circled in FIG. 11, magnetoplasticity has been demonstrated.

FIG. 12 shows an array of nanoindents performed in the Example below, on the shaded face of material such as that show by force F in FIG. 4a.

FIGS. 13 (13a and 13b) show results from nanoindentation experiments of the Example below.

DETAILED DESCRIPTION OF THE PREFERRED EMBODIMENTS

Referring to the figures, there are shown several, but not the only, embodiments of the invented devices and methods.

The present invention makes use of two effects of materials with mobile twin boundaries, and, specifically, of magnetoplastic and/or magnetoelastic materials, including materials from the following subsets of magnetoplastic and/or magnetoelastic: magnetic shape memory alloys (MSMA, which are ferromagnetic or "magnetic"); materials resulting from martensitic transformation (typically called "martensite"); and other providers of twins.

Magnetoplasticity/magnetoelasticity is the magnetic-field-induced deformation enabled through the magnetic-field-induced displacement of crystallographic twin boundaries. Deformation-induced-change of magnetization occurring in magnetoplastic/magnetoelastic materials has been demonstrated by Mullner et al. (Müllner P, Chernenko V A, Kostorz G, Scripta Mater 2003b; 49:129). The strain-induced change of magnetization due to twin rearrangement is the reverse/inverse effect to magnetoplasticity. With regard to applications for magnetoplasticity, the present inventors believe that magnetoplasticity is relevant for actuators, whereas the inverse/reverse effect is relevant for sensors and/or power generation. Numerous publications deal with many aspects of the ferromagnetic martensites in Ni—Mn—Ga

alloys such as martensitic transformations and martensite structure (e.g. Chernenko et al. 1995), magnetic-field-induced deformation (e.g. Murray et al 2000a, Sozinov et al 2002) and the associated magneto-stress (Chernenko et al. 2000, Mullner et al. 2002, Tickle and James 1999, Chernenko et al. 1999, Murray et al. 2000b). However, only few results concerning the inverse/reverse effect (strain-induced change of magnetization) have so far been published (Mullner et al 2003b, Soursa et al 2004a, Soursa et al 2004b, Straka et Heczko 2006).

The magnetoplastic effect is related to the magnetic-field-induced displacement of twin boundaries, which is a thermodynamically irreversible process (Ullakko 1996, Mullner et al. 2002). On the microscopic scale, a twin boundary moves by the motion of twinning disconnections (Pond and Celotto 2002), a process which can be triggered by a magnetic force on the dislocation (Mullner and Ullaklco 1998, Ferreira and Vander Sande 1999, Mullner 2006). In Ni_2MnGa, the cooperative motion of twinning dislocations finally leads to a strain of up to 10% (Müllner et al. 2004a).

FIG. **1** shows the setup of the experiment with which deformation-induced change of magnetization was demonstrated. A magnetoplastic material in form of a parallelepiped (1) is fixed between two pressure pistons (2) that introduce the load. Two quartz glass push rods (3) transmit the displacement of the top and bottom surfaces of the sample/pistons to the extensometers (not shown on the figure). A Hallbach cylinder (cylindrical permanent magnet, 4) produces the magnetic field H_x (large arrow). A Hall probe (5) measures the sum of H_x and stray field H_S (small arrows) on the side surface of the sample. The difference between measured field and H_x is taken as a measure for the sample magnetization in the direction indicated by the arrows.

Referring to FIG. **1**, uniaxial compression experiments under orthogonal magnetic field were done on a single crystal with composition $Ni_{51}Mn_{28}Ga_{21}$ (numbers indicate atomic percent). The sample was cut as a rectangular prism with {100} faces in all directions and measured 5.45(2) mm×3.26(2) mm×2.34(2) mm. In the ferromagnetic austenitic phase, i.e. above the reverse transformation temperature of 316 K, the sample was a single crystal with the ordered cubic $L2_1$ structure. At room temperature, the material is in the martensitic phase. The crystallographic directions a and c of all twin variants were parallel within 3° to the sample edges. The easy magnetization axis is parallel to the c direction.

The sample was deformed in uniaxial compression and unloaded at constant speed (2×10^{-6} m/s) in a mechanical testing machine equipped with a 500 N load cell and extensometers insensitive to magnetic fields. The magnetic field $\lambda_0 H$=0.7 T was produced by a permanent magnet system. The sample was mounted in such a way that the longest edge was parallel to the compression axis (z direction). The x direction was defined parallel to the shortest edge of the sample; x-y-z constitute Cartesian coordinates. The magnetic field was applied in x direction. A Hall probe was positioned close to one of the sample surfaces which were parallel to the y-z plane. The set-up of the experiment is outlined in FIG. **1**.

FIG. **2** shows stress (squares) and magnetization (triangles) as a function of compressive deformation along <100> direction of a $Ni_{51}Mn_{28}Ga_{21}$ (numbers indicate atomic percent) single crystal measured at constant orthogonal magnetic field of 0.7 T along the x direction. Open and full symbols indicate values for increasing and decreasing deformation along the z direction. Upon deformation, the stress increases quickly to about 1.5 MPa at 0.04% strain. Above 0.1% strain, stress increases slowly and almost linearly up to 1.9% strain. At larger strain, stress increases rapidly again. Upon unloading,

the total strain is recovered, however at a lower stress level compared with loading. The magnetization along the x axis (divided by its value M_0 in the undeformed state) decreases linearly with increasing deformation up to 1.9%. Upon unloading, the magnetization restores its initial value with a small hysteresis.

FIG. **2** shows the results of the experimentation represented by FIG. **1**. Upon mechanical loading along the z direction at constant speed, the stress increases strongly at the beginning. The slope of the stress-strain curve decreases rapidly right after the onset of plastic deformation and is almost constant up to about 1.9% compressive strain and a corresponding stress of 6 MPa. At larger strain, the stress increases more rapidly. Over the whole deformation range, the relative magnetization in x direction M_x/M_{x0}=$(H-H_x)(H_0-H_c)$ (H and M are the field detected with the Hall probe and the magnetization of the sample, H_0 and M_0 are the values in the undeformed state) decreases within experimental error linearly with increasing strain. Upon unloading, the stress decreases rapidly at the beginning and more slowly with decreasing strain until the full deformation is recovered. The relative magnetization increases again linearly until it reaches the initial value. The magnetization exhibits a negligible hysteresis. The slopes of the magnetization curves in both directions of deformation are constant and equal within experimental error over a wide range of strain whereas the stress curves have different shapes.

FIG. **3** is a schematic of the magnetization process through deformation in magnetoplastic martensitic materials. (a) Dark and bright gray indicate two twin variants. The local magnetization (arrows) aligns with the easy axis that is differently oriented for each twin variant. (b) Under an applied magnetic field H_x, the twin boundaries move causing growth of the twin variants with c parallel to the field. In the other twin variants, the magnetic moments rotate towards the direction of the magnetic field. (c) Under an applied load (F_z), the twin boundaries move causing growth of one twin variant with the crystallographic c axis parallel to the load direction and shrinkage of the other. The specimen deforms since the crystallographic axes c<a. At the same time, the distribution of magnetic moments changes and alters the total magnetization.

The twin rearrangement due to the action of a magnetic field and a mechanical force and the associated processes of deformation and magnetizing on the mesoscopic scale are shown schematically in FIG. **3**. In the undeformed state and without magnetic field (FIG. **3**a), the twin structure contains self-accommodated elastic domains with the crystallographic c directions distributed irregularly. In the absence of 180° magnetic domains (which is always true for magnetic fields of 0.1 T and larger and even, in some cases, without application of a magnetic field), there is a considerable stray-field H_S caused by domains with the axis of easy magnetization (which is parallel to the c direction) perpendicular to the surface.

In the schematic of FIG. **3**, only one martensite domain with one set of twins is present. Such a structure can be obtained after a suitable magnetic or mechanical treatment. In the present study, there are many martensite domains with differently oriented sets of twins.

When a magnetic field H_x>>0.1 T is applied along the x direction, the twin boundaries move in such a way that the twins with c parallel to the x direction grow at the expense of twins with c perpendicular to the x axis (FIG. **3**b). In regions, through which a twin boundary passes, the c direction switches from parallel to the z axis to parallel to the x axis. Since c/a<1, the sample shrinks along the x direction and

expands along the z direction (magnetoplasticity). In addition to the motion of twin boundaries, the magnetic field H, causes the magnetic moments in the domains with c perpendicular to the x direction to rotate by an angle θ with sin θ=H_x/H_A (H_A is the saturation field) towards the x direction (FIG. **3**b). In the present experiment, H_x/H_A≅0.7 and θ≅45°. Owing to the rotation of the magnetic moments, the stray-field increases. The Hall probe (FIG. **1**) detects the sum of the stray-field and the applied field.

When the sample is mechanically compressed along the z direction, the twin boundaries move in the opposite direction, i.e. the twins with c parallel to the z direction grow at the expense of twins with c perpendicular to the z axis (FIG. **3**c). In regions, through which a twin boundary has passed, the c direction switched from parallel to the x axis to parallel to the z axis. Thereby, the direction of the magnetic moments rotates from parallel to the x axis to about 45° inclined to the x axis. This causes a reduction of the stray field which is detected by the Hall probe. Very close to the sample surface, the magnetic induction originating from the stray field is a linear function of the fractions of each twin variant. Since the strain is a linear function of the twin variant fractions, too, the signal of the Hall probe decreases linearly with strain (FIG. **2**). Upon mechanical unloading, the reverse process occurs. The twin boundaries move again under the action of the magnetic field H_x until the twin pattern and the shape of the unloaded state (FIG. **3**b) are reached. Since in the present experiments, strain and magnetization are controlled by the fractions of twin variants, there is no significant hysteresis between loading and unloading curves (FIG. **2**).

The role of the magnetic bias field (H_x in the above experiment) is twofold. First, the bias field removes all 180° domain boundaries and causes a net magnetization M_x in x direction. This component of the magnetization induces voltage in the coil, for extraction of electrical power. Second, the magnetic bias field works against the applied force and restores the shape of the magnetoplastic and/or magnetoelastic material after removal of the force. The restoration of the shape implies a further change of magnetization capable of generating electrical power. Below a bias field comparing to the saturation field (about 1 T for Ni₂MnGa), the recoverable strain decreases and vanishes below a threshold field (see Mullner et al. 2002). Alternatively, or additionally, restoration of the initial state may also be achieved through the application of a bias stress, for example, by a lever system forcing the shape of the magnetoplastic and/or magnetoelastic material back to the same or generally the same shape as the initial state.

FIG. **4** shows a sample geometry and indentation pattern/physical contour. (a) The parallelepiped-shaped sample was compressed along the direction parallel to its shortest edge while heated and cooled. Cartesian coordinates are defined on the sample as indicated. In most of the volume, the crystallographic c direction was parallel to the x axis. There are two possibilities for the orientation of the crystallographic a and b directions. (b) Schematic of the surface structure with bands/indentation pattern indicated.

A Ni₅₀Mn₂₉Ga₂₁ (numbers indicate atomic percent) single crystal was grown following the Bridgman method with a rate of 3.5 mm/h. A sample was cut using electric discharge erosion forming a parallelepiped with faces parallel to cubic {001} planes. The composition was measured using x-ray fluorescence analysis and energy-dispersive x-ray analysis with transmission and scanning electron microscopes. The composition varied by a couple of percent across the crystal. Electron diffraction revealed the presence of 14M (orthorhombic) and 10M (tetragonal) martensite with the 14M mar-

tensite being predominant. The dimensions of the sample were 5.4 mm×4.0 mm×2.0 mm. Cartesian coordinates are defined on the sample (sample coordinates) such that the shortest, intermediate, and longest edges are parallel to the x, y, and z directions. The crystal was annealed at 800° C. for one hour under an inert argon atmosphere. One surface with dimensions 5.4 mm×2.0 mm was polished with 1 μm diamond slurry (light gray shaded face in FIG. **4**). After polishing, the sample was compressed with forces parallel to the x direction (i.e. parallel to the shortest edges, see FIG. **4**a) to a stress level of 12±2 MPa and heated to 150° C. During the heating and cooling period, the force was held constant until the sample reached ambient temperature. The stress of 12 MPa applied during the heat treatment is sufficient to align the crystallographic c direction with the loading direction (see e.g. Müllner et al. 2004b). Thus, the crystallographic c direction which is the shortest lattice parameter must be parallel to the x direction in most of the sample. For the crystallographic a and b directions, there are two possibilities as indicated in FIG. **4**a.

A Veeco Dimension 3100 Atomic Force Microscopy (AFM) System was used to characterize the relief of the surface and the magnetic structure of the surface. Surface reliefs were taken in tapping mode with a diamond tip with tip radius 25±3 nm and an apex angle of 60°. For the magnetic-force microscopy (MFM) experiments, a ferromagnetic tip with a Co-coating and magnetization parallel to the tip axis (i.e. perpendicular to the investigated surface) was used. The magnetic tip is particularly sensitive for variations to out-of-plane magnetization.

Long, straight thin bands parallel to the edges were found on the polished surface (FIG. **4**b). The bands were identified as twins (see below). The experiments were terminated when an accidental collision of the AFM with the sample surface occurred. After the collision, the twin boundaries have moved and the twins have thickened considerably.

After the thermo-mechanical treatment, the polished surface displayed an almost periodic pattern of thin criss-crossing bands parallel to the sample edges. FIG. **4**b is a schematic of the polished surface with "long" twins (i.e. twins parallel to the long edge of the sample which is the z direction) shaded gray and "short" twins (i.e. twins parallel to the short edge of the sample) shaded black.

FIG. **5** is a section of the surface relief of the shaded face in FIG. **4**a, wherein the image is produced by atomic force microscopy (AFM). The surface relief contains terraces separated by slopes stemming from twins, which are the bands in FIG. **4**b. FIG. **5** is a surface relief taken with the AFM in tapping mode. The surface shows terraces separated by inclined slopes. The root mean square surface roughness is 8 nm.

FIG. **6** shows how the twin crystallography is identified. (a) Cross-section of a twin parallel to the z direction. The orientation of each twin variant is indicated. (b) Cross-section of a twin parallel to the x direction. (c) Example of a AFM surface profile used for evaluating the relief angles ϕ_a and ϕ_c. The slope angles ϕ_a and ϕ_c (defined in FIG. **6**a,b) were evaluated from surface profiles (e.g. FIG. **6**c) and are ϕ_a=3.0°±0.3° and ϕ_c=4.3°±0.5°. The slope angles are related to the lattice parameters by

$$\varphi_a = \arctan\frac{b}{c} - \arctan\frac{c}{b} \qquad (6a)$$

-continued

$$\varphi_c = \arctan\frac{a}{b} - \arctan\frac{b}{a} \qquad (6b)$$

where the orientation of the crystallographic directions is given in FIGS. **6**a and b. There are, in principal, many possibilities for the arrangement of twins and the orientation of the crystallographic directions in each twin. However, the crystallographic c direction was oriented by applying a normal stress of 12 MPa along the x direction (FIG. **4**a). Thus, the predominant lattice parameter parallel to the x direction in the crystal must be the c lattice parameter which is the shortest.

FIG. **7** shows the crystallography and nomenclature of twin variants. Orientation and gray scale corresponds to FIG. **1**b. Lower case a, b and c indicate the orientation of the crystallographic directions. Capital letters mark the crystallographic direction perpendicular to the surface and give the variants the name. Since the slope angle for an ac twin (with the b direction parallel to the twin boundary) is more than 6° (assuming c/a=0.9), the presence of ac twins is excluded. The only combination of crystallographic orientations is a∥z, b∥x, and c∥y (B variant, since b is perpendicular to the surface) in the largest regions, a∥z, b∥y, and c∥x (C variant) in the long twins, and a∥x, b∥z, and c∥y (A variant) in the short twins (FIG. **7**).

FIG. **8** shows results of magnetic-force microscopy (MFM) on the same area as displayed as relief in FIG. **5**. FIG. **8**(a) is a MFM image of the area shown in FIG. **5**. The C variants appear as dark lines indicating strong interaction with the MFM tip and out-of-plane magnetization. The A and B variants are hardly distinguishable. Domains are elongated along the crystallographic c direction. FIG. **8**(b) is a magnified view of an area similar to FIG. **8**(a) indicating an interaction of the domains across twin boundaries.

FIG. **8**a is an MFM image of the same area as shown in FIG. **5**. The strong contrast in the two horizontal stripes along the z direction indicates out-of-plane magnetization in the long twins. For these twins, the crystallographic c direction is perpendicular to the surface (C variants), i.e. parallel to the x direction (compare FIG. **7**). The crystallographic c direction is the direction of easy magnetization (Sozinov and Ullakko 2002). The regions with the A and B variants (FIG. **5**) display a weak magnetic contrast in form of long stripes. FIG. **8**b is a magnified view of FIG. **8**a also containing regions with A, B and C variants. FIG. **8**b was taken with higher magnetic sensitivity compared to FIG. **8**a. The stripes are parallel to they direction which is parallel to the crystallographic c direction in both A and B variants (FIG. **7**).

For a cubic-to-orthorhombic martensite transformation, there are six orientation variants in the martensitic phase. Each variant has six {110}<1$\bar{1}$0> twinning systems; two of each ab-, bc-, and ac-twin type (Müllner et al. 2004b, Müllner et al. 2005). Thus, there are 36 possible twinning systems not including twins forming within twin variants. It is remarkable that given one known crystallographic direction in the predominant martensite variant, which in the present case is c, the analysis of the surface profile yields the complete crystallography of all twin variants. Thus, crystallographic orientation and spatial configuration of the twin structure can be fully characterized by AFM alone without employing diffraction methods.

The identification of the A, B, and C variants and the orientation of the twin boundaries prove the presence of ab-twins and bc-twins. For ab-twins (bc-twins), the twin boundary contains the crystallographic c (a) direction. It may be noted that the stress induced by the AFM accidentally impact-

ing the sample (as described above) was sufficient to move the twin boundaries. Thus, ab-twins and bc-twins are very mobile. The present results substantiate the idea that different twinning modes are active in orthorhombic Ni—Mn—Ga MSMA resulting in a variation of the magnetic-field-induced strain.

The magnetic-force microscopy images reveal a strong signal for the C variants. Since the magnetization of the MFM tip is perpendicular to the surface, a strong signal indicates an out-of-plane magnetization, which is parallel to the crystallographic c direction. The c direction is the direction of easy magnetization in orthorhombic Ni—Mn—Ga martensite (Sozinov and Ullakko 2002). Thus, the conclusion that the C variant has out-of-plane magnetization is consistent with the magnetic properties of the material. The magnetic contrast in A and B variants reveals magnetic domains which are elongated along the crystallographic c direction. The width of the magnetic domains is the same for A and B variants. This indicates that magnetic domains have a rod-like shape. The domains match across twin boundaries (FIG. **6**b) to ensure magnetic compatibility by avoiding magnetic charges on the twin boundaries (Vlasova et al. 2000). Similar magnetic domain structures were reported for tetragonal Ni—Mn—Ga martensite (Ge et al. 2004, Pan and James 2000, Sullivan and Chopra 2004).

Thus, it has been shown above on macroscopic samples that it is possible to control the magnetic and crystallographic states of a magnetoplastic material through the application of magnetic fields and/or mechanical forces. This represents one embodiment of a writing process. It has also been shown that it is possible to read the state of individual twin domains through the use of atomic force microscopy and magnetic force microscopy. A schematic of apparatus and methods of writing on (W, here a mechanical force F) and reading of (R, here apparatus for atomic force or magnetic force microscopy) a macroscopic portion of multi-state material is shown in FIG. **9**. While FIG. **9** portrays a mechanical force for W, it will be understood from this disclosure and from FIG. **1** that a magnetic-field-change system may also be used for the writing system W.

With current micro-fabrication tools, micro- and nano-pillars with diameters of 100 nm and below can be produced. For instance, gold pillars with thickness between 100 nm and 200 nm were recently produced, mechanically deformed using a nanoindenter and characterized (Greer et al. 2005). Thus, the writing method outlined above and depicted in FIGS. **1** and **2** may directly be downscaled to the nano- and micro-scales.

One embodiment of the system uses mechanical force with or without combined use of magnetic field to write the "bits" on/in magnetoplastic and/or magnetoelastic material. We do not use "bit" in this disclosure to refer to the traditional meaning referring to binary coding, but, instead, we use it for convenience to refer to the multi-state elements of embodiments of the present invention, wherein said multi-states preferably comprise greater than two states, and more preferably six or more for a single magnetoplastic/magnetoelastic element. Likewise, the term "element" is not intended to refer to elements of the Periodic Table, but rather individual pieces/portions/regions (for example, individual memory units) according to the invention that are preferably formed/defined by pieces/portions/regions of magnetoplastic/magnetoelastic material.

One embodiment of the system uses a reading process that may be achieved through a combination of atomic-force microscopy and magnetic-force microscopy; diffraction-based work/reading is not required in preferred embodiments.

In other embodiments, reading is accomplished through other means including optical interferometry, spin-polarized scanning electron microscopy, the magneto-optical Kerr effect, and/or combination of such methods.

One example, of how multi-functionality of the embodiments of the invention may be used, is as follows: one functionality may comprise the shape state serving as the main actuation function such as positioning a probe or defining a memory. Simultaneously, another functionality may be provided, for example, the magnetic state providing a signal to indicate the current position. In this embodiment, displace function and indicate function are combined in one material. Other embodiments combine other operations such as read & write, sense & indicate, sense & control, for example.

Preferred Materials:

The materials used for the preferred multi-state memory and multi-functional devices are those which couple magnetic and crystallographic/shape states. The preferred materials are those with mobile twin boundaries, wherein strain-induced deformation/change in said twin boundaries produces change in magnetization, and wherein magnetic-field change produces deformation/change in the twin boundaries (the later being the feature that is typically implied by the terms "magnetoplasticity" or "magnetoelasticity."). Therefore, the preferred materials used for the multi-state memory and/or multi-functional devices of the invention may be selected from the broad categories of magnetoplastic and magnetoelastic materials, including from the following subsets of magnetoplastic and/or magnetoelastic: magnetic shape memory alloys (MSMA, which are ferromagnetic or "magnetic"); materials resulting from martensitic transformation (typically called "martensite"); and other providers of twins. The terms "magnetoplastic" and "magnetoelastic" overlap to some extent, in that "magnetoelastic" is commonly used even for some materials that do exhibit hysteresis.

The phrases "magnetplasticity/magnetoelasticity" and "magnetoplatic/magnetoelastic materials" as applied in embodiments of the invention do not necessarily include all ferromagnetic materials, for example, these phrases preferably do not include "classical" magnetostriction (magnetostricitive materials). Whereas current magnetostrictive materials are limited to a maximum of about 0.2% strain (for Terfenol-D), the preferred megnetoplastic/megnetoelastic materials exhibit typically above 1% strain, and, in some embodiments, up to about 10% strain and possibly more.

Further, the magentoplastic/magnetoelastic materials used in preferred embodiments of this invention are not piezoelectric. However, the inventors envision that there may be materials developed or discovered in the future that are both magentoplastic/magnetoelastic and piezoelectric, and, hence, could be included in the preferred embodiments. The inventors envision that materials may be recognized or discovered in the future that are magnetoplastic/magnetoelastic and piezoelectric, and that may offer more memory states (electrical states) and also more actuation options (namely electrical field) for switching from one state to another (control).

Requisite for magnetoplasticity is the magnetic-field-induced motion of twin boundaries. This requisite implies the following properties:

(i) The material must deform more easily by twinning than by dislocation motion.

(ii) The twinning stress must be less than the magnetostress τ_M, i.e. the stress which can be induced through a magnetic field.

Factors affecting (i) above include the crystal structure (trend: lower symmetry is better than higher symmetry), the

lattice potential (trend: strong bonding is better than weak bonding), the size of the lattice parameter (trend: larger is better than smaller). Factors affecting (ii) include the magnetic anisotropy constant K (the higher the better) and the twinning shear (the smaller the better).

Regarding applications, a large strain might be desirable. This implies a large twinning shear, which is in conflict with (ii). Furthermore, it is desirable to obtain magnetoplasticity with a small magnetic field. This implies a large saturation magnetization M_s. Thus, the desired materials properties are:

1. Large magnetic anisotropy K.
2. Large saturation magnetization M_s.
3. For large stress output: small twinning shear.
4. For large strain output: large twinning shear.

Regarding memory applications of preferred embodiments of the invention, a large strain output is important; however, the requirement that the stress required for twinning must be smaller than the magnetostress still holds. The multi-state data storage medium according to preferred embodiments of the invention should be material with the basic properties (i), (ii), and (1-4) above, and may be manufactured as solid bulk part, as thin film, as nanostructured bulk part, as nanostructured thin film, as nano-columns and in any other shape and form. Nano-structured arrays of the material may be of particular interest as the bit size can be tailored in this case using nano-fabrication methods.

FIG. 10 summarizes magnetic and magneto-mechanical properties of some (potentially) ferromagnetic materials. Materials in FIG. 10 for which magnetoplasticity has been reported in the literature are circled. Embodiments of the invention may include one or more of the materials in FIG. 10, with values surrounded by a rectangle being least favorable, and values surrounded by a triangle being most favorable. The strain $\epsilon_{M,max}$ is proportional to the twinning shear and marks the theoretical maximum of magnetic-field-induced strain. The saturation field $\mu_0 H_a$ is the magnetic field at which the maximum magnetostress $\tau_{M,max}$ is reached. Further increase of the magnetic field does not increase the magnetostress.

Current research in the field of magnetoplasticity focuses on ferromagnetic shape-memory alloys (MSMA), because in these materials, the twinning stress is very low. Particular attention is being paid to Heusler alloys, particularly off-stoichiometric Ni_2MnGa. Other ferromagnetic shape-memory alloys (i.e. non-Heusler alloys) which are under study include FePd, CoPt, FePt, and Fe_3Pd. Recently, magnetoplasticity was reported for an antiferromagnetic (AFM) magnetic shape-memory alloy γ-Mn—Fe—Cu (J. H. Zhang, W. Y. Peng, S. Chen, T. Y. Hsu (X. Zaoyao), Appl. Phys. Lett. 86, 022506 (2005)). Non-shape-memory alloys which have been studied in context of magnetoplasticity include dysprosium and τ-MnAl—C.

FIG. 11 lists and categorizes many magnetoplastic and potentially magnetoplastic materials, as well as citations to scientific literature discussing these materials. Embodiments of the invention may include one or more of the listed materials and/or one or more materials selected from the broad categories of materials. For materials that are circled in FIG. 11, magnetoplasticity has been demonstrated. The citations in FIG. 11 are:

| [Cui 2004] | J. Cui, T. W. Shield, R. D. James, Acta mater. 52, 35 (2004). |
| [Fujita 2000] | A. Fujita, K. Fukamichi, F. Gejima, R. Kainuma, K. Ishida, Appl. Phys. Lett. 77, 3054 (2000). |

-continued

[James 1998]	R. D. James and M. Wuttig, Phil. Mag. A 77, 1273 (1998).
[Kostorz 2005]	G. Kostorz and P. Müllner, Z. f. Metallk. 96, 703 (2005).
[Lieb. 1976]	H. H. Liebermann and C. D. Graham, Jr. Acta Met. 25, 715 (1976).
[Santa. 2006]	R. Santamarta, E. Cesari, J. Font, J. Muntasell, J. Pons, J. Dutkiewicz, Scripta Mater. 54, 1985 (2006).
[Solo. 2004]	A. S. Sologubenko, P. Müllner, H. Heinrich, K. Kostorz, Z. f. Metallk. 95, 486 (2004).
[Vlasova 2000]	N. I. Vlasova, G. S. Kandaurova, N. N. Shchegoleva, J. Magn. Magn. Mater. 222, 138 (2000).
[Wada 2003]	T. Wada, T. Tagawa, M. Taya, Scripta Mater. 48, 207 (2003).
[Wuttig 2001]	M. Wuttig, J. Li, C. Craciunescu, Scripta Mater. 44, 2393 (2001).
[Zhang 2005]	J. H. Zhang, W. Y. Peng, S. Chen, T. Y. Hsu (X. Zaoyao), Appl. Phys. Lett. 86, 022506 (2005).

As may be seen from the above comments and FIGS. 10 and 11, preferred materials may be selected from the group consisting of: Heusler shape-memory alloy, non-Heusler ferromagnetic shape-memory alloy, antiferromagnetic shape-memory alloy, non-shape-memory magnetoplastic alloy, Ni_2MnGa, Dy, α-Fe, Co—Ni, τ-MnAl—C, $L1_0$ FePd, $L1_0$ CoPt, $L1_0$ FePt, Ni_2MnGa, Co_2NiGa, Ni_2MnAl, Ni_2FeGa, Fe_3Pd, Fe—Pd—PT, γ-Mn—Fe—Cu, $Ni_{51}Mn_{28}Ga_{21}$, Ni—Mn—Ga alloys, Ni—Mn—Ga ferromagnetic martensite, and combinations thereof. Especially-preferred for nonvolatile memory embodiments will be materials, including materials selected from the broad category of magnetoplastic/magnetoelastic and from the above list, that exhibit magnetic and crystallographic states that are stable without the use of an external electrical input or other force.

Discussion of Features and Advantages of Preferred Embodiments

Current conventional device, logical and memory technology is based on binary elements. On the other hand, elements, according to embodiments of the invention, made of magnetic shape-memory material have six crystallographic states. The crystallographic states are linked to three magnetic states. This enables the combined usage of a single element as memory and logic unit. As a consequence, the low-level programming of computers becomes much more efficient. Because a single element may have six states, memory density increases 3 fold.

Current memory devices including dynamic random access memory (DRAM) are based on volatile mechanisms. Those mechanisms depend on the permanent supply of power. When power fails, data is lost. The multi-state memory of preferred embodiments of the invention may be based on materials, from the broad category of magnetoplastic/magnetoelastic materials, selected for exhibiting magnetic and crystallographic states that are stable without the use of an external force (e.g., external electric field); such multi-state memory may, therefore, be non-volatile

Embodiments of the present invention may continue the historic trend toward functionalities being carried by materials rather than by machine parts. Further, embodiments of the invention, by providing multiple functions from one material, may reduce the complexity of systems which may lead to an increase of performance, miniaturization, and lowering of costs.

EXAMPLE

The following is an example comprising study and analysis of material, and comprising writing and reading methods of

the multi-states of said material, that may be applied to one, but not the only, embodiment of the invention.

Atomic-force microscopy, magnetic-force microscopy (MFM), and nanoindentation experiments were performed on a Ni—Mn—Ga single crystal with orthorhombic (14M) martensite. The surface relief was characterized and used to identify the orientation of individual twin variants. It was shown that ab- and bc-twinning modes are present. The magnetic domains are elongated along the crystallographic c direction. Twin variants with the c direction perpendicular to the surface exhibit an out-of-plane magnetization which can be identified through a strong contrast in the MFM image. The deformation caused with nanoindentation is recoverable to a large degree. No trace of deformation twinning was found after unloading. The results are discussed in the light of pseudo-elastic twinning and dislocation activity. It is concluded that although the residual deformation is due to dislocation activity, it is likely that pseudo-elastic twinning took place during loading and unloading. The results indicate a size effect on deformation twinning under localized loading.

1. Introduction

Magnetic shape-memory alloys (MSMA) are distinguished from other ferromagnetic materials by the coupling mechanism between shape and magnetization. Large (uniaxial) magnetic anisotropy constant and mobile twin boundaries are at the origin of large magnetic-field-induced deformation (magnetoplasticity). Plastic (i.e. irreversible) strains up to 10% have been reported for off-stoichiometric Ni_2MnGa Heusler alloy single crystals (see e.g. references [1-4], below). The reverse effect or deformation-induced change of magnetization requires a magnetic field bias to minimize demagnetizing by the formation of 180° domains (references [5-7]).

There are various ideas for applications of MSMA. For instance, actuator applications including stepper motors, pumps, valves and devices for surgery make use of the "direct" effect of magnetic-field-induced deformation. Sensor applications make use of the "reverse" effect or deformation-induced change of magnetization. In all application, considerable magnetic fields need to be produced. Devices involving MSMA transducers in the millimeter size range and larger may require considerable power. In addition, losses from induction limit the actuation frequency of large systems. That these obstructions are reduced when the scale is smaller provides motivation for miniaturization. However, mechanical properties change dramatically when objects are small (at least in one direction) compared to a characteristic length specific for a certain deformation mechanism [reference 8], and the yield stress may increase strongly with decreasing size [reference 9]. Thus the investigation of mechanical properties on the micrometer and smaller scales is needed for the development of miniaturized applications.

The micromechanism of magnetoplasticity is the motion of twinning disconnections [references 10-14]. Disconnections are interfacial line defects with elastic fields (displacement, strain and stress) identical to the elastic fields of dislocations. Greer et al. [reference 9] assume that the efficiency of dislocation multiplication decreases with decreasing size of single crystalline gold columns with diameter below 1 μm. Lack of dislocations is the reason for the high yield strength of these gold columns when only a few hundred nanometer in diameter.

Whether such observations apply to twinning in magnetic shape-memory alloys and what limits magnetic-field-induced twinning and deformation-induced change of magnetization at small length scale are open questions. The present paper reports on an investigation of two questions, (i) whether

it is possible to locally induce deformation twinning with a sharp tip thereby inducing a magnetic signature which can be identified with magnetic-force microscopy (MFM) and (ii) if there is a size effect on the deformation mechanisms which are triggered due to localized loading.

2. Magnetoplasticity

2.1 Micromechanism of Magnetoplasticity

The magnetoplastic effect is related to the magnetic-field-induced displacement of twin boundaries. On the microscopic scale, a twin boundary moves by the motion of twinning disconnections [references 10-16], a process which can be triggered by a force on the disconnection. A disconnection is an interfacial line defect with a dislocation component and a step component. A disconnection is characterized by a line vector (which is parallel to the interface), a step vector (which is perpendicular to the interface) and a Burgers vector (which is of arbitrary direction). For a twinning disconnection, the Burgers vector is parallel to the interface. The motion of a twinning disconnection is conservative and compares to glide of a lattice dislocation.

The Burgers vector defines the deformation carried by a moving disconnection. Thus, the dislocation component controls the interaction of a stress field with the disconnection. A shear stress τ exerts a mechanical force F_{mech} on a disconnection:

$$F_{mech} = \tau b \qquad (1)$$

where b is the magnitude of the Burgers vector. The step vector defines the volume which is transformed by a moving disconnection. Thus, the step component controls the interaction of a magnetic field with the disconnection. For a material with uniaxial magnetic anisotropy K, the magnetic force F_{mag} exerted by a magnetic field on the disconnection was derived in [reference 12]. In the special case where the magnetic field is parallel and perpendicular to the easy axis of magnetization of the twinned crystals sharing the interface, the magnetic force is

$$F_{mech} = \begin{cases} \mu_0 MHd\left(1 - \dfrac{\mu_0 MH}{4K}\right) & \text{for } H \le H_A \\ Kd & \text{for } H \ge H_A \end{cases} \qquad (2)$$

where μ_0 is the free space permeability, M is the saturation magnetization, H is the magnetic field, d is the step height of the disconnection, and $H_A = 2K/\mu_0 M$ is the saturation field. Equating mechanical and magnetic force yields the magnetostress which is the mechanical stress that is produced by a magnetic field. The maximum magnetostress is the ratio K/s where s=b/d is the twinning shear.

2.2 Twin-surface Interaction

When a twin grows from a surface into a crystal, the energy increases as a result of three factors: the growing interface, the growing strain field and, if the material is ferromagnetic, the demagnetizing field. The energy contribution of the twin boundary is proportional to the interface area whereas the work done by the growing twin is proportional to the twinned volume, the twinning shear and the applied stress. Therefore, the shear stress r required to grow the twin decays with increasing twin thickness t:

$$\tau = \frac{\alpha \gamma_{tb}}{st} \qquad (3)$$

where α is a geometrical factor on the order of unity, γ_{tb} is the twin boundary energy, and s is the twinning shear.

The disconnections experience an image force due to the dislocation component. The image force is inversely proportional to the distance from the surface and tends to pull dislocations out of the crystal (e.g. reference [17]). When a deformation twin is formed from a surface and grows into the crystal, the twin disappears after unloading if the image force on each dislocation is larger than the force due to internal stresses. This effect may be called elastic twinning [reference 18] or pseudo-elastic twinning. Pseudo-elastic twinning was observed by Garber in calcite in the late 1930s. Garber published his observations in Russian. Garber's results were reviewed in English by Kosevich [reference 18]. Pseudo-elastic twinning requires stress concentrations on the surface [reference 18].

The energy contribution due to the reorientation of the axis of easy magnetization depends on the magnetic domain structure and the relative sizes of twin and magnetic domains. If a magnetic field larger than the saturation field is applied, the magnetic effects on twin growth are limited to the magnetic force on twinning disconnections, Eq. (2). The same is true for a moderate magnetic field as long as the field is large enough to remove 180° domain boundaries. For weak magnetic fields, the reorientation of the axis of easy magnetization may result in localized magnetic domains with out-of-plane magnetization. These domains have a strong magnetic field with large energy. This energy provides a further driving force for detwinning after unloading and may contribute to pseudo-elastic twinning.

2.3 Twin-interface Interaction

Interfaces interrupt the slip plane (which for twinning disconnections is the twinning plane) and, thus, determine the free path of twinning disconnections. Interfaces themselves do not have long-range stress field. Therefore, a 'first' twinning disconnection that approaches a 'defect free' interface (i.e. an interface that does not already contain a twinning disconnection) moves under the action of a magnetic or mechanical force until it is blocked by the interface. The stress field of the blocked dislocation obstructs the motion of the second twinning disconnection. A critical mechanical or magnetic stress τ_c is required, to push the second disconnection into the interface. The critical stress is inversely proportional to the total number N=d/t of twinning disconnections [references 19, 20]:

$$\tau_c = \frac{Gd}{4\sqrt{2}\,(1-\nu)t} \qquad (4)$$

where G and v are the shear modulus and Poisson's ratio, d and t are the d-spacing of twining planes and the twin thickness. For very small twins (e.g. t=10 nm) the critical shear stress τ_c is about 10^{-2} G, which is two orders of magnitude larger than the magnetostress. Thus, the second disconnection of a thin twin does not reach the interface. For very thick twins (e.g. t=100 μm) the critical shear stress τ_c is about 10^{-6} G, which is a factor of 30 less than the magnetostress. Thus, the second, third and following disconnections reach the interface and form a nascent dislocation wall. As the dislocation wall grows, the more disconnection that are pushed into the interface, the stronger is the repulsive force that these disconnection exert on a incoming disconnections. The fraction η of twinning disconnections that form a disconnection wall in an interface can be approximated as [references 14, 20, 21]:

$$\eta = 1 - \sqrt{2}\, s \frac{\tau_c}{\tau} \qquad (5)$$

where $\tau(>\tau_c)$ is the resolved shear stress on the twinning plane in the twinning direction.

A dislocation wall is a mechanically stable dislocation configuration. Dislocations are trapped in a dislocation wall. It therefore requires a force to remove a dislocation from a wall. This force increases with increasing wall size and causes hysteresis [reference 13].

3. Experiments

A $Ni_{50}Mn_{29}Ga_{21}$ (numbers indicate at. %) single crystal was grown following the Bridgman method with a rate of 3.5 mm/h. A sample was cut using electric discharge erosion forming a parallelepiped with faces parallel to cubic {001} planes. The composition was measured using x-ray fluorescence analysis and energy-dispersive x-ray analysis with transmission and scanning electron microscopes. The composition varied by a couple of percent across the crystal. Electron diffraction revealed the presence of 14M (orthorhombic) and 10M (tetragonal) martensite with the 14M martensite being predominant. The dimensions of the sample were 5.4 mm×4.0 mm×2.0 mm. Cartesian coordinates are defined on the sample (sample coordinates) such that the shortest, intermediate, and longest edges are parallel to the x, y, and z directions. The crystal was annealed at 800° C. for one hour under an inert argon atmosphere. One surface with dimensions 5.4 mm×2.0 mm was polished with 1 μm diamond slurry (light gray shaded face in FIG. 4a). After polishing, the sample was compressed with forces parallel to the x direction (i.e. parallel to the shortest edges, see FIG. 4a) to a stress level of 12±2 MPa and heated to 150° C. During the heating and cooling period, the force was held constant until the sample reached ambient temperature. The stress of 12 MPa applied during the heat treatment is sufficient to align the crystallographic c direction with the loading direction (see e.g. reference [4]). Thus, the crystallographic c direction which is the shortest lattice parameter must be parallel to the x direction in most of the sample. For the crystallographic a and b directions, there are two possibilities as indicated in FIG. 4a.

FIGS. 4a and b: Sample geometry and indentation pattern. (a) The parallelepiped-shaped sample was compressed along the direction parallel to its shortest edge while heated and cooled. Cartesian coordinates are defined on the sample as indicated. In most of the volume, the crystallographic c direction was parallel to the x-axis. There are two possibilities for the orientation of the crystallographic a and b directions. (b) Schematic of the surface structure with bands.

A Veeco Dimension 3100 Atomic Force Microscopy (AFM) System was used to characterize the relief and the magnetic structure of the surface and to perform nanoindentation experiments. Surface relief were taken in tapping mode with a diamond tip with tip radius 25±3 nm and an apex angle of 60°. For the nanoindentation experiments, diamond tip, cantilever and photo detector were calibrated using a sapphire single crystal. The tip was pressed onto the sapphire surface up to a load corresponding to a photo detector reading of 2 V. Up to this load, the diamond tip did not indent the sapphire surface. For the magnetic-force microscopy (MFM) experiments, a ferromagnetic tip with a Co-coating and magnetization parallel to the tip axis (i.e. perpendicular to the investigated surface) was used. The magnetic tip is particularly sensitive for variations to out-of-plane magnetization.

Long, straight thin bands parallel to the edges were found on the polished surface (FIG. 4b). In the regions bound by the thin bands and within the bands themselves, arrays of nanoindentation experiments were performed. FIG. 12 shows an array of indents. Each triangular shaped indent is surrounded by pileups of displaced or deformed material. In each line of 10 experiments, the maximum applied load increase from right to left from a photo detector reading of 0.2 V (corresponding to 6.1 μN) in increments of 0.2 V to a maximum reading of 2.0 V (corresponding to 61 μN). The bands were identified as twins (see paragraph 4). Indents were set at least 1 μm apart from each other and also from the nearest twin boundary. In a second series, the distance from the nearest twin boundary was varied from indenting on the boundary to a distance of more than 1 μm. Magnetic-force microscopy images were taken of some of the indents which resulted from loading up to a photo detector reading of 2 V.

FIG. 12: Array of nanoindents performed on the shaded face in FIG. 4a. The indents to the outermost right (barely visible) were obtained with loading to a maximum detector voltage of 0.2 V corresponding to 6.1 μN. The maximum load increases from indent to indent towards the left by 6.1 μN and measures 61 μN for the indents on the outermost left.

The experiments were terminated when an accidental collision of the AFM with the sample surface occurred. After the collision, the twin boundaries have moved and the twins have thickened considerably.

4. Results

After the thermo-mechanical treatment, the polished surface displayed an almost periodic pattern of thin crisscrossing bands parallel to the sample edges. FIG. 4b is a schematic of the polished surface with "long" twins (i.e. twins parallel to the long edge of the sample which is the z direction) shaded black and "short" twins (i.e. twins parallel to the short edge of the sample) shaded gray. FIG. 5 is a surface relief taken with the AFM in tapping mode. The surface shows terraces separated by inclined slopes. The root mean square surface roughness is 8 nm. The slope angles ϕ_a and ϕ_c (defined in FIGS. 6a and b) were evaluated from surface profiles (e.g. FIG. 6c) and are $\phi_a = 3.0° \pm 0.3°$ and $\phi_c = 4.3° \pm 0.5°$. The slope angles are related to the lattice parameters by

$$\varphi_a = \arctan\frac{b}{c} - \arctan\frac{c}{b} \qquad (6a)$$

$$\varphi_c = \arctan\frac{a}{b} - \arctan\frac{b}{a} \qquad (6b)$$

where the orientation of the crystallographic directions is given in FIG. 6a,b.

FIG. 5: Surface relief of the shaded face in FIG. 4a. The surface relief contains terraces separated by slopes stemming from twins, which are the bands in FIG. 4b.

FIG. 6: Schematic of twin crystallography. (a) Cross-section of a twin parallel to the z direction. The orientation of each twin variant is indicated. (b) Cross-section of a twin parallel to the x direction. (c) Example of a surface profile used for evaluating the relief angles ϕ_a and ϕ_c.

There are, in principal, many possibilities for the arrangement of twins and the orientation of the crystallographic directions in each twin. However, the crystallographic c direction was oriented by applying a normal stress of 12 MPa along the x direction (FIG. 4a). Thus, the predominant lattice parameter parallel to the x direction in the crystal must be the c lattice parameter which is the shortest. Since the slope angle for an ac twin (with the b direction parallel to the twin bound-

ary) is more than 6° (assuming c/a=0.9), the presence of ac twins is excluded. The only combination of crystallographic orientations is a||z, b||y, and c||x (B variant, since b is perpendicular to the surface) in the largest regions, a||z, b||x, and c||y (C variant) in the long twins, and a||y, b||z, and c||x (A variant) in the short twins (FIG. 7).

FIG. 8a is an MFM image of the same area as shown in FIG. 5. The strong contrast in the two horizontal stripes along the z direction indicates out-of-plane magnetization in the long twins. For these twins, the crystallographic c direction is perpendicular to the surface (C variants), i.e. parallel to the y direction (compare FIG. 7). The crystallographic c direction is the direction of easy magnetization [reference 3]. The regions with the A and B variants (FIG. 7) display a weak magnetic contrast in form of long stripes. FIG. 8b is a magnified view of FIG. 8a also containing regions with A, B and C variants. FIG. 8b was taken with higher magnetic sensitivity compared to FIG. 8a. The stripes are parallel to the y direction which is parallel to the crystallographic c direction in both A and B variants (FIG. 7).

FIG. 7: Crystallography and nomenclature of twin variants. Orientation and gray scale corresponds to FIG. 4b. Lower case a, b, and c indicate the orientation of the crystallographic directions. Capital letters mark the crystallographic direction perpendicular to the surface and give the variants the name.

FIGS. 8a and b: Magnetic-force microscopy. (a) MFM image of the area shown in FIG. 5. The C variants appear as dark lines indicating strong interaction with the MFM tip and out-of-plane magnetization. The A and B variants are hardly distinguishable. Domains are elongated along the crystallographic c direction. (b) Magnified view of an area similar to (a) indicating an interaction of the domains across twin boundaries.

FIG. 13a displays the results of the nanoindentation experiments. Triangles, squares and circles refer to experiments in A, B, and C variants. Open symbols indicate the indentation depth at full load whereas full symbols indicate the residual indentation depth after unloading. The indentation depth at full load increases almost linearly for all variants. The depth is deepest in the B variants and least deep in the A variants. The same trend is observed for the depth of the residual indent. However, the depth of the residual indent amounts to only about 30% of the depth at maximum load. The results of indentation experiments at different distances from the twin boundaries were identical within experimental error. FIG. 13b is the stress versus indentation depth diagram for the B domain. The stress represents a normalized value obtained from dividing the applied load by the area of the indent. The stress is initially very large and decreases with increasing depth.

FIGS. 13 A and B: Results from nanoindentation experiments. (a) Indentation depth vs. maximum load. The open symbols represent the depth at maximum load; the full symbols mark the residual depth after unloading. Triangles, squares and circles indicate results from A, B, and C variants. The depth at maximum load increases nearly linearly with maximum applied load. The indentation depth in C variants is systematically larger than the depth in B and A variants. The residual deformation is smallest for A variants and about the same for B and C variants. (b) Data of B variants evaluated for stress vs. indentation depth. With increasing depth the average stress under the indenter decreases.

5. Discussion

For a cubic-to-orthorhombic martensite transformation, there are six orientation variants in the martensitic phase. Each variant has six $\{110\}<1\overline{1}0>$ twinning systems; two of

each ab-, bc-, and ac-twin type [references 4,13]. Thus, there are 36 possible twinning systems not including twins forming within twin variants. It is remarkable that given one known crystallographic direction in the predominant martensite variant, which in the present case is c, the analysis of the surface profile yields the complete crystallography of all twin variants. Thus, crystallographic orientation and spatial configuration of the twin structure can be fully characterized by AFM alone without employing diffraction methods.

The identification of the A, B, and C variants and the orientation of the twin boundaries prove the presence of ab-twins and bc-twins. For ab-twins (bc-twins), the twin boundary contains the crystallographic c (a) direction. The stress induced by the AFM accidentally impacting the sample was sufficient to move the twin boundaries. Thus, ab-twins and bc-twins are very mobile. It was suggested in [reference 4] that different twinning modes are active in orthorhombic Ni—Mn—Ga MSMA resulting in a variation of the magnetic-field-induced strain. The present results substantiate that suggestion.

The magnetic-force microscopy images reveal a strong signal for the C variants. Since the magnetization of the MFM tip is perpendicular to the surface, a strong signal indicates an out-of-plane magnetization, which is parallel to the crystallographic c direction. The c direction is the direction of easy magnetization in orthorhombic Ni—Mn—Ga martensite [reference 3]. Thus, the conclusion that the C variant has out-of-plane magnetization is consistent with the magnetic properties of the material. The magnetic contrast in A and B variants reveals magnetic domains which are elongated along the crystallographic c direction. The width of the magnetic domains is the same for A and B variants. This indicates that magnetic domains have a rod-like shape. The domains match across twin boundaries (FIG. 8b) to ensure magnetic compatibility by avoiding magnetic charges on the twin boundaries [reference 22]. Similar magnetic domain structures were reported for tetragonal Ni—Mn—Ga martensite [references 23-25].

The results of the indentation experiments show that after unloading only about 30 percent of the total deformation remains. Permanent (plastic) deformation may be due to twinning or dislocation activity. Twinning causes reorientation of the lattice. In the A and B variants, twinning would produce C variants. C variants can be identified by MFM imaging via their strong signal stemming from out-of-plane magnetization (FIG. 8a). For most of the indents, the MFM signal did not displayed variation compared with the surrounding area. This indicates that the residual deformation was carried by lattice dislocations. This is an interesting result since in uniaxial compression tests, twinning occurs in this material at only a few MPa stress [references 4,5] whereas yielding by dislocation motion requires a much higher stress level [reference 26]. Furthermore, under uniform loading, Hensler alloys tend to fail by brittle fracture [reference 26].

In nanoindentation experiments, the applied average stress under the tip area is largest at the beginning of the indentation since the area is very small. At a 10 nm indentation depth, the average normal stress at the surface is about 10 GPa (FIG. 8b). This is an enormous stress level. Thus, the stress near the surface might be sufficient to grow a twin. However, the stress field extends into the material only by about three times the indentation depth and decays very rapidly beyond that [reference 27]. Therefore, if a twin forms, it can grow only to a length of about three times the indentation depth. At this short distance, the interaction of the twinning disconnections with the surface is still strong. Upon unloading, the image force causes detwinning (i.e. pseudo-elastic twinning). This

assumption follows Garber's conclusion (see discussion in reference [18]) that pseudo-elastic twinning requires stress concentrations while homogeneous loading leads to permanent twinning. Following this line of thought, the stress distribution caused by the accidental impact by the AFM covered a large enough area to cause permanent (plastic) twinning. One might conclude that with increasing indenter tip size and tip radius, there should be a transition from pseudo-elastic twinning to plastic twinning. Tall et al. [reference 28] indeed reported indentation-induced permanent twinning in LaAlO$_3$ using a microindenter. This indicates a size-effect on the deformation mechanisms operating under localized loading, which might be investigate using tips with different tip radii [reference 29].

About 70 percent of the deformation is recovered. It is unlikely, however, that 70 percent of the deformation is purely elastic. The recovery of deformation may stem from pseudo-elastic twinning or from the recovery of dislocations due to the image force. Dislocations contribute at least partially to deformation. This follows from highly localized deformation in the pileups next to the indents, which by far exceeds the twinning shear. Thus, dislocation motion is required to form pileups. However, the intensive and irreversible mutual interaction of dislocations prevents full recovery of the deformation after unloading [reference 30]. Thus, the large recoverable deformation is an indication that pseudo-elastic twinning took place.

6. Conclusions

The crystallography and spatial configuration of twinning systems can be characterized by using AFM provided a limited knowledge about the orientation state of one martensite variant.

Different twinning modes are active in orthorhombic Ni—Mn—Ga martensite. The ab- and bc-twinning modes were identified.

Magnetic domains in orthorhombic Ni—Mn—Ga martensite have the shape of rods elongated along the crystallographic c direction.

C variants are magnetized perpendicular to the surface and cause a strong stray-field leading to strong interaction with an MFM tip.

After nanoindentation about 70 percent of the deformation recovers. The residual deformation is carried by dislocation activity.

It is likely that pseudo-elastic twinning takes place during nanoindentation.

The results indicate a size-effect on twinning deformation under localized loading.

References

[1] K. Ullakko, J. K. Huang, C. Kantner. R. C. O'Handley, V. V. Kokorin, J. Appl. Phys. 69 (1996) 1966.

[2] R. C. O'Handley, J. Appl. Phys. 83 (1998) 3263.

[3] Sozinov, K. Ullakko, IEEE Trans. Magn. 38 (2002) 2814.

[4] P. Müllner, V. A. Chemenko, G. Kostorz, J. Appl. Phys. 95 (2004) 1531.

[5] P. Müllner, V. A. Chemenko, G. Kostorz, Scripta Mater. 49 (2003) 129.

[6] L. Straka, O. Heczko, Scripta Mater. 54 (2006) 1549.

[7] G. Li, Y. Liu, B. K. A. Ngoi, Scripta Mater. 53 (2005) 829.

[8] E. Arzt, Acta Mater. 46 (1998) 5611.

[9] J. R. Greer, W. C. Oliver, W. D. Nix, Acta Mater. 53 (2005) 1821.

[10] R. C. Pond, P. J. Hirth, Solid State Physics, 47 (1994), 287-365.

[11] R. C. Pond, S. Celloto, Int. Mater. Rev. 48 (2003) 225.

[12] P. Müllner, V. A. Chernenko, M. Woligarten, G. Kostorz, J. Appl. Phys. 92 (2002) 6708.

[13] P. Müllner, D. Mukherji, R. Erni, G. Kostorz, Proc. Int. Conf. "Soid to solid phase transformations in inorganic materials" PTM'05, Phoenix, Ariz., Mai 29-Jun. 3, 2006, Vol. 2, pp 171.

[14] P. Müllner, Int. J. f. Mater. Res. (formerly Z. f. Metallk.) 97 (2006) 205.

[15] G. Kostorz, P. Müllner, Z. f. Metallk. 96 (2005) 703.

[16] S. Rajasekhara, P. J. Ferreira, Scsripta Mater. 53 (2005) 817.

[17] J. P. Hirth and J. Lothe, "Theory of dislocations", 2nd Ed., Krieger, Malabar Fla.1992 pp. 86.

[18] A. M. Kosevich, Soy. Phys. Usp. 14 (1971) 286.

[19] P. Müllner, C. Solenthaler, Phil. Mag. Lett. 69 (1994) 111-113.

[20] P. Müllner, C. Solenthaler, Phil. Mag. Lett 69 (1994) 171-175.

[21] S. V. Kamat, J. P. Hirth, P. Müllner, Phil. Mag. A 73 (1996) 669-680.

[22] N. I. Vlasova, G. S. Kandaurova, N. N. Shchegoleva, J. Magn. Magn. Mater. 222 (2000) 138.

[23] Y. Ge, O. Heczko, O. SŘderberg, V. K. Lindroos, J. Appl. Phys. 96 (2004) 2159.

[24] M. R. Sullivan, H. D. Chopra, Phys. Rev. B 70 (2004) 094427.

[25] Q. Pan, R. D. James, J. Appl. Phys. 87 (2000) 4702.

[26] F. Xiong, Y. Liu, E. Pagounis, J. Magn. Magn. Mater. 285 (2005) 410.

[27] N. Schwarzer, G. M. Pharr, Thin Solid Films 469-470 (2004) 194.

[28] P. D. Tall, C. Coupeau, J. Rabier, Scripta Mater. 49 (2003) 903.

[29] Z. Xue, Y. Huang, K. C. Hwang, M. Li, J. Eng. Maer. Techn. 124 (2002) 371.

[30] C. R. Taylor, E. A. Stach, G. Salamo, A. P. Malshe, Appl. Phys. Lett. 87 (2005) 073108.

Some embodiments may be described as follows: The preferred system controls and detects the crystallographic state of a non-cubic crystal. Said crystallographic state may be connected/related to a magnetic state and/or to a shape state. Said crystallographic state may be controlled by a magnetic field and/or by a mechanical force field and/or an A/C electric field. The crystal may be a magnetic shape-memory alloy. The crystal may be magnetically and structurally anisotropic, and the magnetic and crystallographic anisotropy coupled. Said magnetic state may be controlled by a mechanical action. The magnetic state and/or the crystallographic state may be detected with the magneto-optical Kerr effect. The magnetic state and/or the crystallographic state may be detected with spin-polarized electrons. The magnetic state and/or the crystallographic state may be detected with optical interferometry, or with other or a combination of methods/effects. A system may be provided wherein two different states/functionalities selected from said magnetic states, crystallographic states, and shape states are simultaneously used as read and write operators. Two different states/functionalities may be selected from said magnetic state, crystallographic state, and shape state, said two different states/functionalities that are selected may be simultaneously used as sense and indicate operators. Two different states/functionalities selected from said magnetic state, crystallographic state, and shape state may be simultaneously used as sense and control operators. Said magnetic states and/or crystallographic states and/or shape states may be embodied in crystal attached to or grown on a substrate. Said magnetic state and/or crystallographic state and/or shape states may be embodied in individual bits/elements embedded in a crystal.

In some embodiments, a system for writing and reading data comprises control and detection of crystallographic states of a magnetic shape-memory alloy or other magnetoplastic and/or magnetoelastic material. Said crystallographic state may be connected/related to a magnetic state and/or to a shape state. Said crystallographic state may be controlled by a magnetic field and/or by a mechanical force field and/or an A/C electric field. The crystal may be magnetically and structurally anisotropic and the magnetic and crystallographic anisotropy are coupled. Said magnetic state may be controlled by a mechanical action. The magnetic state and/or the crystallographic state may be detected with the magneto-optical Kerr effect. The magnetic state and/or the crystallographic state may be detected with the spin-polarized electrons. The magnetic state and/or the crystallographic state may be detected with optical interferometry. The magnetic state and/or the crystallographic state may be detected with other methods than mentioned above. The magnetic state and/or the crystallographic state may be detected with a plurality/combination of effects selected from the group consisting of: magneto-optical Kerr effect, spin-polarized electrons, and interferometry. The magnetic state and/or the crystallographic state is detected with a plurality/combination of effects selected from the group consisting of: magneto-optical Kerr effect, spin-polarized electrons, interferometry, and other effects not including diffraction-based methods. The system may be further adapted for sense&indicate functionality, and/or further adapted for sense&control functionality. Embodiments of the invention may comprise methods of writing and reading data/information comprising use of any of the systems described herein; and/or methods of sensing and indicating data/information comprising use of any of the systems described herein. In preferred embodiments of the apparatus, systems, and methods, said crystal comprises at least six crystallographic states. Preferably, said crystal father comprises multiple magnetic states.

Although this invention has been described above with reference to particular means, materials, and embodiments, it is to be understood that the invention is not limited to these disclosed particulars, but extends instead to all equivalents within the broad scope of the following claims.

The invention claimed is:

1. A logic or memory device comprising a magnetoplastic and/or magnetoelastic material having at least six states selected from the group consisting of magnetic states, crystallographic states, and shape states.

2. A device as in claim 1 which is a combined logic and memory device.

3. A device as in claim 2 wherein the memory is nonvolatile.

4. A device as in claim 1, wherein said material is magnetic shape memory alloy.

5. A device as in claim 1, wherein said material is selected from the group consisting of: Heusler shape-memory alloy, non-Heusler ferromagnetic shape-memory alloy, antiferromagnetic shape-memory alloy, non-shape-memory magnetoplastic alloy, Ni_2MnGa, Dy, α-Fe, Co—Ni, τ-MnAl—C, Ll_0FePd, Ll_0CoPt, Ll_0FePt, Ni_2MnGa, Co_2NiGa, Ni_2MnAl, Ni_2FeGa, Fe_3Pd, Fe—Pd-PT, γ-Mn—Fe—Cu, $Ni_{51}Mn_{28}Ga_{21}$, Ni—Mn—Ga alloys, Ni—Mn—Ga ferromagnetic martensite, and combinations thereof.

6. A device as in claim 1 that is a data reading and writing device.

7. A device as in claim 1 that is a displacement and sensing device.

8. A device as in claim 1 that is a sensing and control device.

9. A device as in claim 1 that is a sensing and indicating device.

10. A device as in claim 1, wherein two of said at least six states are read and write operators.

11. A device as in claim 1, wherein two of said at least six states are sense and indicate operators.

12. A device as in claim 1, wherein two of said at least six states are sense and control operators.

13. A sensor, actuator, logic or memory device comprising a ferromagnetic, non-cubic crystal having multiple crystallographic states relating to magnetic states, and wherein said device comprises means for controlling, and means for detecting, said multiple crystallographic states, wherein said means for controlling is selected from a group consisting of a magnetic field, a mechanical force, and an A/C electric field.

14. A device as in claim 13 wherein said crystallographic states are related to shape states.

15. A device as in claim 13 wherein said means for controlling is a magnetic field.

16. A device as in claim 13 wherein said means for controlling is a mechanical force.

17. A device as in claim 13 wherein said means for controlling is an A/C electric field.

18. A device as in claim 13, wherein said crystal is a magnetic shape-memory alloy.

19. A sensor, actuator, logic or memory device comprising a ferromagnetic crystal having multiple crystallographic states, wherein said crystal is magnetically and crystallographically anisotropic and the magnetic and crystallographic anisotropy are coupled, and wherein said device comprises means for controlling said multiple crystallographic states, and wherein said means for controlling is selected from a group consisting of a magnetic field, a mechanical force, and an A/C electric field.

20. A device as in claim 13 wherein said means for detecting comprises detection using the magneto-optical Kerr effect.

21. A device as in claim 13, wherein said means for detecting comprises detection with spin-polarized electrons.

22. A device as in claim 13, wherein said means for detecting comprises detection with optical interferometry.

23. A device as in claim 13, wherein said crystal is attached to or grown on a substrate.

24. A logic or memory device comprising a magnetoplastic and/or magnetoelastic material having at least six states selected from the group consisting of magnetic states, crystallographic states, and shape states, and wherein two different states selected from said at least six states are simultaneously used as operators selected from the group consisting of read and write operators, sense and indicate operators, and sense and control operators.

25. A device as in claim 24, wherein magnetoplastic and/or magnetoelastic material comprises a crystal attached to or grown on a substrate.

26. A method comprising writing data on an element and reading the data, the element comprising a magnetoplastic and/or magnetoelastic material having at least six states selected from the group consisting of magnetic states, crystallographic states, and shape states, wherein said writing comprises a step selected from the group consisting of applying a magnetic field change and applying a mechanical force to said material, and said reading the data comprises a step selected from the group consisting of atomic-force microscopy, magnetic-force microscopy, spin-polarized electrons, magneto-optical Kerr effect, and optical interferometry.

27. A method of providing logic or memory comprising displacing twin boundaries of a magnetoplastic and/or mag-

netoelastic material and detecting the displacement of said twin boundaries, said displacing comprising a step selected from the group consisting of applying a magnetic field change and applying a mechanical force to said material, and said detecting comprising a step selected from the group consisting of atomic-force microscopy, magnetic-force microscopy, spin-polarized electrons, magneto-optical Kerr effect, and optical interferometry, the method further comprising using

said displacing and detecting for operations selected from the group consisting of reading and writing, sensing and indicating operators, and sensing and controlling.

28. A method as in claim **27**, wherein said magnetoplastic and/or magnetoelastic material has at least six states comprising magnetic states, crystallographic states, and shape states.

* * * * *